Mars Express

Solar Corona Experiment:

A Cookbook

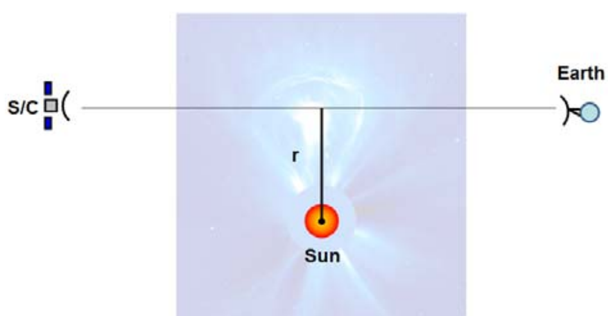

Mars Express Radio Science

MaRS

Reference:

Issue:	2
Revision:	1
Date:	17. Mar. 2014

Prepared by:

Stefan Remus

European Space Agency, ESAC, Villanueva de la Canada, Spain

Co-Authors:

M. Hahn[1], M. Bird[2], M. Paetzold[1], B. Haeusler[3], S. Asmar[4], O. Witasse[5] and G.L. Tyler[6]

[1] Rheinisches Institut für Umweltforschung, Abt. Planetenforschung, Cologne, Germany
[2] Argelander-Institut für Astronomie, Universität Bonn, Bonn, Germany
[3] Institut für Raumfahrttechnik, Universität der Bundeswehr München, Neubiberg, Germany
[4] Jet Propulsion Laboratory, Caltech, Pasadena, CA, USA
[5] European Space Agency, ESTEC, Keplerlaan 1, 2200 AG Noordwijk, The Netherlands
[6] Center for Radar Astronomy, Stanford University, Stanford, CA, USA

PAGE LEFT FREE

1 Document Administration

1.1 Content

1 DOCUMENT ADMINISTRATION ... 4

1.1 CONTENT ... 4
1.2 DISTRIBUTION LIST ... 5
1.3 DOCUMENT CHANGE RECORD ... 5
1.4 APPLICABLE DOCUMENTS ... 6
1.5 REFERENCED DOCUMENTS ... 6
1.6 TABLE OF FIGURES ... 10
1.7 ABBREVIATIONS ... 12

2 INTRODUCTION ... 14

2.1 PURPOSE ... 14
2.2 SCOPE ... 14
2.3 LIST OF REFERENCE DOCUMENT ... 14

3 THE SOLAR CORONA OBSERVATION ... 15

3.1 THE PRINCIPLE ... 15
3.2 OBSERVABLES ... 16
3.3 DETERMINABLE PHYSICAL QUANTITIES OF THE SCO EXPERIMENT ARE: ... 16
3.3.1 Total electron content (Ranging) ... 16
3.3.2 Change of TEC (Doppler) ... 19
3.4 CORONAL ELECTRON DENSITY ... 20
3.5 CORONAL MASS EJECTIONS (CMEs) ... 22
3.6 SEPARATION OF UP- AND DOWNLINK FREQUENCY SHIFTS DUE TO THE PLASMA CONTRIBUTION ON THE RECORDED RADIO SIGNAL ... 27
3.7 FURTHER STUDIES ON SOLAR CORONA DATA ... 28
3.7.1 Scintillation ... 28
3.7.2 Spectral Analysis ... 28
3.7.3 Ephemerides Calculation ... 28

4 DESCRIPTION OF A SCO PSA DATA SET ... 28

4.1 MEX ARCHIVE ACCESS ... 28
4.2 ROS ARCHIVE ACCESS ... 32
4.3 NASA PDS ARCHIVE ... 34
4.4 DESCRIPTION OF THE DATA LEVELS ... 34
4.5 OPEN LOOP AND CLOSED LOOP DATA ... 38
4.6 BRIEF EXPLANATION ON RANGING AND DOPPLER TRACKING DATA ... 39
4.7 LEVEL 2 DATA CALIBRATION: DIFFERENTIAL DOPPLER ... 39
4.8 LEVEL 2 DATA CALIBRATION: RESIDUAL CALIBRATED FREQUENCY SHIFTS (COLUMN 12 OF THE LEVEL 2 DATA) ... 40
4.9 RANGING CALIBRATION ... 40
4.10 OVERLAY OF DOPPLER AND RANGING TEC RESULTS (CALCULATION OF TEC_0) ... 41
4.11 LIST OF REFERENCE DOCUMENTS ... 41
4.12 SOFTWARE ... 41

5 DATA PROCESSING ... 41

5.1 EXAMPLE 1: PLANE OF SKY PLOT ... 41
5.2 EXAMPLE 2: EARTH ATMOSPHERE CORRECTION ... 42
5.3 EXAMPLE 3: TEC PLOT ... 43
5.4 EXAMPLE 4: CORONAL ELECTRON DENSITY PLOT ... 44

APPENDICES ... 46

1.2 Distribution List

Recipient	Institution	No. of copies

1.3 Document Change Record

Issue	Rev.	Section	Date	Changes	Author
1.0	0	all	14.03.2013	All	SR
1	1	3.6	27.03.2013	Chapter 3.6 changed to a separated chapter 4 and the chapter 4 became chapter 5	SR
		New 4.8		Summary of RS and FD steps structured and partially rewritten	
		4.10		Chapter added	
		In front of Appendices		Acknoledgement added	
1	2	3.5	08.04.2013	Last paragraph included (procedure to derive the difference between the downlink paths)	SR
		1.1 & 1.6	15.04.2013	Update of the lists	
		Fig. 8		Update of the figure	
		Fig. 9		Fig. 9 and a short explanation inserted	
2	0	1.4, 3.1	21.10.2013	AD.6 added	SR
		2.2		Changed partially	
		Chap. 1 - 4		Some wording	
		3.5		Whole chapter got a revision. The proposed velocity determination was wrong	

		4.8		revised	
2	1	all	11.03.2014	Wording and structure figures and tables	SR

1.4 Applicable Documents

	Reference Number	Title	Issue	Date
AD 01	810-005, Rev.E	DSMS Telecommunication Link Design Handbook, 203 Sequential Ranging		Nov. 2000
AD 02	ESA PSS-04-104	Ranging standard Vol.1	2	1991
AD 03	820-013, Deep Space Mission System (DSMS), External Interface Specification, JPL D-16765	0159-Science Radio Science Receiver Standard Formatted Data Unit (SFDU)	draft	February 5. 2001
AD 04	820-013, Deep Space Mission System (DSMS), External Interface Specification, JPL D-16765	TRK-2-18, Tracking System Interfaces, Orbit Data File Interface	3	June 15. 2000
AD 05	IFMS_OCCFTP.PDF	IFMS-OCC interface /MakaluMedia/MR/IFMS/ICD/FTP-OCC	11.4.0	09.Aug.2006
AD 06	ECSS-E-ST-50-05C	European Cooperation for Space Standardization, Space Engineering, Radio Frequency and Modulation	Rev.1	06.Mar.2009

1.5 Referenced Documents

Reference Number, Author, Publisher	Title	Date
RD 01 MEX-MRS-IGM-DS-3036, Issue 1	IFMS Ranging Processing and Calibration Software: Level 1 and Level 2	23.05.2005
RD 02 MEX-MRS-IGM-DS-3035, Issue 5	IFMS Doppler Processing and Calibration Software: Level 1a and 2 Software Design Specification	26.07.2005
RD 03 MEX-MRS-IGM-DS-3038, Issue 4	DSN ODF (Orbit Data File) Calibration Software: Doppler Level 1b to Level 2 Software Design Specification	05.Apr.2007
RD 04 MEX-MRS-IGM-IS-3016, ROS-RSI-IGM-IS-3087, VEX-VRA-IGM-IS-3009, Issue 12, Rev 13	Radio Science File Naming Convention And Radio Science File Formats	24.06.2011

RD 05 Trevor Morley, Frank Budnik; , International Symposium on Space Flight Dynamics, ISSFD 2009	Mars Express and Venus Express Range Residuals for Improving Planetary Ephemerides	28.Sep.2009
RD 06 R. Wohlmuth, I. Plettemeier, P. Edenhofer, M.K. Bird, S.W Asmar	Analysis of Galileo Doppler Measurements during the Solar Occultation in 1994 and 1995	1997
RD 07 S. Baumbach, Astronomische Nachrichten, Band 263, Nr. 6294	Strahlung, Ergiebigkeit und Elektronendichte der Sonnenkorona	1937
RD 08 Allen C. W., Communicated by the Commonwealth Astronomer	Interpretation of Electron Densities from Corona Brightness	May 1947
RD 09 Tyler G.L., JGR, Vol.82, No.28	The Viking Solar Corona Experiment	30 Sep. 1977
RD 10 Muhleman D.O., The Astrophysical Journal, 247, 1093-1101	Solar Wind Electron Densities From Viking Dual-Frequency Radio Measurements	1. Aug. 1981
RD 11 M. K. Bird, Space Science Reviews 33, 99-126,	Coronal Investigations with Occulted Spacecraft Signals,	1982
RD 12 Ho C. M., Pham T.T., DSN Telecommunication Link Design Handbook 810 – 005, 106, Rev B	Solar Corona and Solar Wind Effects	30. Sep. 2010
RD 13 Anderson J. D., JPL D-18609, Interoffice Memorandum, Pasadena, California	Corona Model For ODP	20. Mar. 1997
RD 14 Moyer T D., Monograph 2, Deep Space Communicationand Navigation Series, JPL, California Institute of Technology	Formulation for Observed and Computed Values of Deep Space Network Data Types for Navigation	October 2000
RD 15 Bird M. K., H. Volland, M. Pätzold, P. Edenhofer, S. W. Asmar, J. P. Brenkle, The Astrophysical Journal, 426: 373-381	The Coronal Electron Density Distribution Determined from Dual-Frequency Ranging Measurements During the 1991 Solar Conjunction of the Ulysses Spacecraft	1. May 1994
RD 16 Pätzold M., M.K. Bird, P. Edemhofer, S.W. Asmar, T.P. Mc Elrath; GRL, Vol.22, No. 23, p. 3313-3316	Dual-frequency radio sounding of the solar corona during the 1995 conjunction of the Ulysses spacecraft	1995
RD 17 P.Janardhan, M.K. Bird, P. Edenhofer, R.Wohlmuth, D Plettemeier, S. W. Asmar, M. Pätzold and J. Karl: Solar Physics, 184, 157-172, 1999 Kluwer Academic Publishers	Coronal Velocity Measurements with ULYSSSES: Multi-Link Correlation Studies during two Superior Conjunctions	1997, 1998

RD 18 M. Pätzold, M. Hahn, S. Tellmann, B. Häusler, M. K. Bird, G. L. Tyler, Solar Phys (2012) 279:127–152	Coronal Density Structures and CMEs: Superior Solar Conjunction of Mars Express, Venus Express and Rosetta: 2004, 2006 and 2008	2012
RD 19 MEX_MRS_UBW_TN_3040 , B. Häusler, W. Eidel, D. Hagl, S. Remus, J. Selle, M. Pätzold	Reference Systems and Techniques used for the Simulation and Prediction of Atmospheric and Ionospheric Sounding Measurements at Planet Venus	July 2004
RD 20 M.K. Bird, M. Pätzold, P. Edenhofer, S.W. Asmar, T.P. Mc Elrath, Astronomy and Astrophysics, 316, 441-448	Coronal radio sounding with Ulysses: solar wind electron density near 0.1 AU during the 1995 conjunction	1996
RD 21 B. Bertotti, G. Giampieri, Solar Physics 178, 85-107	Solar Coronal Plasma in Doppler Measurements	1998
RD 22 Giacomo Giampieri, Proceedings of the XI Conference on General Relativity and Gravitational Physics, Trieste (Italy), Sept. 1994	Relativity Experiments in the Solar System	1995
RD 23 A. K. Verma, A. Fienga, J. Laskar, K. Issautier, H. Manche, and M. Gastineau ; Astronomy & Astrophysics manuscript no. Verma˙et˙al	Electron density distribution and solar plasma correction of radio signals using MGS, MEX and VEX spacecraft navigation data and its application to planetary ephemerides	2012
RD 24 Efimov, A. I.; Lukanina, L. A.; Samoznaev, L. N.; Rudash, V. K.; Chashei, I. V.; Bird, M. K.; Pätzold, M.; MEX, VEX, ROS Radio Science Team; Advances in Space Research, Volume 49, Issue 3, p. 500-508	Quasi-periodic frequency fluctuations observed during coronal radio sounding experiments 1991-2009,	2012
RD 25 A. I. Efimov, L. A. Lukanina, L. N. Samoznaev, V. K. Rudash, I. V. Chashei, M. K. Bird, M. Pätzold, and S. Tellmann; AIP Conf. Proc. 1216, pp. 90-93, twelfth international solar wind conference	Quasi periodic Fluctuations Detected in Mars Express Coronal Radio Sounding Observations	2010
RD 26 Tyler G. L., Vesecky J. F., Plume M. A., Howard, H. T., Barnes, A.; The Astrophysical Journal, 249: 318-322	Radio Wave Scattering Observations of the Solar Corona: First-Order Measurements of Expansion Velocity and Turbulence Spectrum using Viking and Mariner 10 Spacecraft	1981
RD 27 Hewish A.; Proc. R. Soc. Lond. A 1955 228, 238-251	The Irregular Structure of the Outer Regions of the Solar Corona	1955

RD 28 Hewish A.; Journal of Atmospheric and Terrestrial Physics; Volume 51, Issues 9–10, p 743–750	A user's guide to scintillation	1989
RD 29 Woo R.; Astrophysics and Space Science 243: 97-104,	Structure in the Solar Corona from Radio Scintillation Measurements	1996
RD 30 ESA SP 1240; ISBN 92-9092-556-6; Authors: Mars Express instrument PIs and ESA scientists	Mars Express – The Scientific Payload	Aug. 2004
RD 31 ESA SP 1291; ISBN 978-92-9221-975-8; Authors: Mars Express instrument PIs and ESA scientists	Mars Express – The Scientific Investigations	June 2009
RD 32 Morley T., Budnik F., Proceedings of the 20th International Symposium on Space Flight Dynamics; (NASA/CP-2007-214158)	Effect on Spacecraft Radiometric Data at Superior Solar Conjunction	2007
RD 33 Morley T., Budnik F., 21st International Symposium on Space Flight Dynamics	Mars Express and Venus Express Range Residuals for Improving Planetary Ephemerides	2009
RD 34 A. Fienga, J. Laskar, T. Morley, H. Manche, P. Kuchynka, C. Le Poncin-Lafitte, F. Budnik, M. Gastineau, and L. Somenzi; Astronomy & Astrophysics 507, 1675–1686	INPOP08, a 4-D planetary ephemeris: from asteroid and time-scale computations to ESA Mars Express and Venus Express contributions	2009
RD 35 B. Hofmann-Wellenhof, H. Lichtenegger, J. Collins; Springer Verlag	Global Positioning System: Theory and Practice; 4th edition	1997
RD 36 M.K. Bird, P. Edenhofer; Physics and Chemistry in Space – Space and Solar Physics, Vol. 20, Physics of the Inner Heliosphere I, Editors: R. Schwenn, E. Marsch; Springer Verlag Berlin Heidelberg;	Chapter 2: Remote Sensing Observations of the Solar Corona,	1990
RD 37 R.De Gaudenzi, E.E.Lijphart, E. Vassallo; IEEE Transactions on Aerospace and Electronic Systems, Vol. 29, No. 1	A New High Performance Multipurpose Satellite Tracking System	Jan. 1993
RD 38 E.K. Smith, R.E. Edelson; JPL Publication 79-117; NASA-CR-163153	Radio Propagation Through Solar and Other Extraterrestrial Ionized Media	Jan. 1980
RD 39 T.A.Croft, W.A. Edson; Radio Science, Volume 17, Number 4, pages 773 – 785	Interplanetary plasma concentration measurements by use of dual frequencies from separated sites	Aug. 1982
RD 40 Tyler G.L.	Private communication	2012

RD 41 V.R. Eshleman, O.K. Garriott, R.L. Leadabrand, A.M. Peterson, H.T. Howard, R.L. Koehler, R.A. Long, B.B. Lusignan; JGR, Vol. 71, No. 13	The Interplanetary Electron Number Density from Preliminary Analysis of the Pioneer 6 Radio Propagation Experiment	1966
RD 42 R.L.Koehler, JGR Space Physics, Vol. 73, No. 15	Radio Propagation Measurements of Pulsed Plasma Streams from the Sun Using Pioneer Spacecraft	1968
RD 43 F. Budnik, T. A. Morley and R.A. Mackenzie; SAO/NASA Astrophysics Data System (ADS)	ESOC's System for Interplanetary Orbit Determination	2004
RD 44 M32ESOCL1B_RCL_030522_00 , PSA archive	MEX Range Calibration	2003
RD 45 M32UNBWL1B_RCL_030801_00, PSA archive	Transponder Gruppenlaufzeit	2003
RD 46 M32ESOCL1B_RCL_021202_00	NNO group delay stability	2002

1.6 Table of Figures

Fig. 1. : SCO experiment: geometry and link configuration overview 15
Fig. 2. : Mars Solar Conjunction 2006 as seen from Earth in the plane of sky (solar ecliptic system). 16
Fig. 3. : Ranging geometry between S/C and G/S. The quantity Δ can be positive or negative. 17
Fig. 4. : Left panel: *TEC* in the x-y plane (solar ecliptic, left subpanel)) and in the x-z plane (solar pole, right subpanel) from RD 11. The lines of constant TEC are given in hexem = 10^{16} el m^{-2}. The plot is based on the model taken from RD 09. Right panel: Some different models for the heliospheric latitude dependency as shown in RD 20. 22
Fig. 5. : Propagation of the CME and the modulated radio signal vs. time. The modulation event at T_0 indicated due to the yellow mark travels along the downlink path indicated by the green mark towards the ground station and indicated by the blue markings upwards to the S/C and then back to the ground station. On that downlink path the CME is sounded again but on a different CME region. This second event is indicated in the drawing with the time T_2'. The details around time T_0 are discussed further. 23
Fig. 6. : Schematic for the position of the signals in space at a defined time T_0 for the up- and downlink. The velocities of the ground station and spacecraft are similar and parallel. The red line indicates all microwave signal positions that were sent in the past from the S/C and the G/S and will arrive in the future at the G/S and the S/C. The yellow markings indicate the positions of the signals that will be received in future. Along the black lines the position is given for the downlink and along the blue lines for the uplink. 23
Fig. 7. : Geometry for the velocity determination of a CME with 2 ground stations 24
Fig. 8. : The 2nd example for the location of the uplink and downlink signals at time T_0. The shown example reflects also the normal case with nonlinear velocity changes between G/S and S/C. The marked example radio signal positions (yellow and blue dots) will only be a bit more twisted in the 3d space. This example shows explicit that the uplink and

downlink modulation does not take place at the same position and due to that also not at the same time as in the 1st example in Fig. 6. 24
Fig. 9. : Location of the CME direction in Space and Time for the general case of different velocity vectors for S/C and G/S. 25
Fig. 10. : Radio signal deflection due to the solar corona on the S- X- and K-Band as shown in RD 21 and RD 22 26
Fig. 11. : ESA archive main search page. The red arrows indicate the menus that are needed for the MEX solar corona data sets search 29
Fig. 12. : Settings for the MEX SCO data sets search: 1 - Data set search/Target Name/Sun, 2 - Mars Express/Instrument/MaRS. 30
Fig. 13. : Execute Query button 30
Fig. 14. : MEX SCO query result: List of observations (datasets) 31
Fig. 15. : ESA archive main search page. The red arrow indicates the tab that is needed for the ROS solar corona datasets search 32
Fig. 16. : Settings for the ROS SCO datasets search. Click on "RSI" and select then the Target Type "Sun". 33
Fig. 17. Execute Query button. 33
Fig. 18. ROS SCO query result: List of observations (data sets) 33
Fig. 19. Part of the aareadme.txt file is shown here as an example. The red circle identifies an SCO data set by the name Solar Conjunction and relates this to the filename of the stored data set. Tthe PDS MEX MaRS web page for the nominal mission lists a directory with the name MEXMRS_0147, which contains a SCO data set. 34
Fig. 20. Screenshot showing parts of the level 1 and 2 SCO dataset structure of the PSA. Left panel reflects the data structure for an observation with an ESTRACK station and the right panel for a DSN pass. The difference in the settings of the receiving stations causes the difference in the level 1 and 2 data structure. 35
Fig. 21. : Level 1a data with a brief column overview. Data descriptions details are given in AD 05. 36
Fig. 22. : Level 1b data with a brief column description. For details see AD 05 36
Fig. 23. : Level 2 DP1 data file content description. For more details go to the corresponding label file. 36
Fig. 24. Level 2 differential Doppler residuals (MEX-X-MRS-1-2-3-EXT2-1623-V1.0\...\DP2\M32ICL2L02_D2X_083120502_00.TAB) 37
Fig. 25. Level 2 residual calibrated frequency shift (MEX-X-MRS-1-2-3-EXT2-1623-V1.0\...\DP2\M32ICL2L02_D2X_083120502_00.TAB) 38
Fig. 26. Level 2 signal level (MEX-X-MRS-1-2-3-EXT2-1623-V1.0\...\DP2\M32ICL2L02_D2X_083120502_00.TAB) 38
Fig. 27. Schematic diagrams for OL (A) and CL (B) data recordings 38
Fig. 28. Example plot for the plane of sky visualization 42
Fig. 29. Level 2 earth atmosphere correction for the frequency residuals. The blue values represent the frequency shift and the red values the path delay change for this 1.5h. (MEX-X-MRS-1-2-3-EXT2-1623-V1.0\...\DP2\M32ICL2L02_D2X_083120502_00.TAB) 43
Fig. 30. Variation of the TEC vs. time. The integrated differential Doppler shows the variation of the total amount of electrons in the path. The absolute value of the column density can only be calculated with differential ranging values. (MEX-X-MRS-1-2-3-EXT2-1623-V1.0\...\DP2\M32ICL2L02_D2X_083120502_00.TAB) 44
Fig. 31. TEC as function of the ray path proximate point distance to the Sun (RD 15). 44
Fig. 32. An example for the electron density as a function of solar distance in sun radii (RD 36). 45
Fig. 33. MEX SCO 2004 plane of sky plot. The position of MEX is shown for each day from the first day of data to the last day. The red dot marks the date of solar conjunction. 46
Fig. 34. MEX SCO 2006 plane of sky plot (similar to Fig. 33). 49
Fig. 35. MEX SCO 2008 plane of sky plot (similar to Fig. 33). 51
Fig. 36. MEX SCO 2010 - 2011 plane of sky plot. The position of MEX is shown for each day in the solar offset range between +/- 40 solar radii. The central red dot marks the date of solar conjunction. 54

FIG. 37. : MEX SCO 2013 PLANE OF SKY PLOT. THE POSITION OF MEX IS SHOWN FOR EACH DAY IN THE SOLAR OFFSET RANGE BETWEEN +/- 40 SOLAR RADII. THE CENTRAL RED DOT MARKS THE DATE OF SOLAR CONJUNCTION. 58
FIG. 38. ROS SCO 2006 PLANE OF SKY PLOT (SIMILAR TO FIG. 33). 59

1.7 Abbreviations

AU	Astronomical Unit
CL	Closed Loop
CME	Coronal Mass Ejection
DSN	Deep Space Network
ESA	European Space Agency
FD	Flight Dynamics
FTP	File Transfer Protocol
G/S	Ground station
Hexem	Unit of Electron Column Density (1 hexem = 1 TEC Unit = 1 TECU =10^{16} electrons/m^2)
IFMS	Intermediate Frequency and Modem System
LOS	Line of Sight
LT	Light time
MaRS	Mars Express Radio Science
MEX	Mars Express
MPTS	Multi Purpose Tracking System
NASA	National Aeronautics and Space Administration
NNO	New Norcia ESA ground station
ODF	Orbit Data File
OL	Open Loop
PDS	Planetary Data System (NASA)
PLL	Phase Lock Loop
PSA	Planetary Science Archive (ESA)
RF	Radio Frequency
RFDU	Radio Frequency Distribution Unit
ROS	Rosetta
RS	Radio Science (team)
RSR	Radio Science Receiver
SCO	Solar Corona Occultation
S/C	Spacecraft
S/N	Signal to Noise ratio
TEC	Total Electron Content
TNF	Tracking Navigation Data File

VEX Venus Express

2 Introduction

The PSA stores data of all experiments performed on ESA planetary missions and makes them available to the public. Many experiments are executed on each mission, each producing many different kinds of raw data that require special calibrations and instrumental knowledge.

Solar corona sounding observations were executed on Mars Express, Rosetta and Venus Express and solar corona occultation (SCO) data from Mars Express and Rosetta are stored in the ESA archive PSA and NASA archive PDS. The SCO data on these missions were collected at ESA and NASA ground station antennas. The ESA NNO 35 m parabolic dish was used as a baseline in most observations, but the higher S/N ratio of the DSN 70 m network allows observing at very close distances of the signal path to the Sun and is therefore used preferentially for coronal radio sounding. During the SCO opportunities, all 3 missions are conducted in dual-frequency mode using S/X- downlinks simultaneously, thereby allowing one to extract the frequency dispersive plasma effects on the ranging tones and carrier frequency of the signals.
The raw data products are different at the NASA and ESA stations due to different receiving systems and configurations. A guide to the different raw data sets and an explanation of the observations are provided in this document, entitled Solar Corona Experiment – A Cookbook.

2.1 Purpose

The main task of this SCO cookbook is to give an introduction to the subject and to enable a smooth and fast transition to a higher level data analysis. Not all aspects of the analysis are discussed in detail but literature is referenced that can be used for further studies.
This cookbook includes an overview of the observables and how they can be used. It also provides a guide to the available data in the archives and how to process the data as an initial step to a more detailed scientific analysis.

2.2 Scope

The document describes the observational methods, the experiment configuration, the operational modes, and initial steps for analysis of the data. Most of the information is also available in the referenced documents that can also be studied in parallel.

Section 3 gives an introduction to the solar corona experiment, identifies and discusses the observables (some in detail when not available in the literature), often providing literature as reference documents.

Section 4 explains how the PSA archive data can be retrieved and discusses some calibration issues. The structure of the data sets is explained and shown in overviews.

Section 5 shows a few example plots derived from the current archive data or, if not available in the archive, from the literature. This section is subject to change in future versions.

The Appendix presents a list of the currently available SCO data sets from the MEX and ROS missions.

2.3 List of reference document

Lists of documents are given in the AD and RD tables. Also the processing relevant documents are part of each dataset of the PSA and can be found in the document folders.

Some general information of the Mars Express mission is also given in the 2 special ESA publications at http://sci.esa.int/ESA_SP-1240 (RD 30) and http://sci.esa.int/ESA_SP-1291 (RD 31).

3 The Solar Corona Observation

3.1 The Principle

The SCO experiment is one component of the Mars Express Radio Science (MaRS) investigation. All radio science experiments on planetary missions take advantage of the radio communication system, consisting of the transponder RF-system on the S/C and the transmit/receive facilities on ground. The use of this equipment implies that the frequencies and are defined by the engineering requirements of the solar system missions themselves. Specific designated frequency bands are reserved for planetary and interplanetary missions (AD 06). The communication systems of the ESA missions Mars Express (MEX), Venus Express (VEX) and Rosetta (ROS) utilize carrier frequencies at S-band (2.1-2.3 GHz) and X-band (7.1 – 8.4 GHz).

The SCO experiment is normally conducted in a 3-way link configuration, a link being any radio connection between S/C and G/S at a defined carrier frequency. Past experiments have used a configuration with an S-band uplink (ground station to spacecraft) and coherent S- & X-band downlinks (spacecraft to ground station). This configuration is more sensitive to electron content changes in the uplink, but it is also more sensitive for multipath effects that can cause loss of the uplink on the S/C. The lesser sensitivity to free electrons at higher frequencies is the reason why the more robust configuration with X-band uplink and S/X-band downlinks was chosen for most SCO observations.

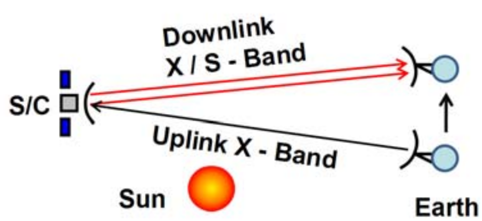

Fig. 1. : SCO experiment: geometry and link configuration overview

Fig. 1 shows the principle for the SCO observation. The SCO measurements for MEX, VEX and Rosetta are planned and executed when the S/C apparent offset from the Sun is within 40 solar radii (solar elongation angle within approx.10°). The view from the Earth is shown in Fig. 2 . Each dot is separated from the previous dot by 1 earth day (24h).

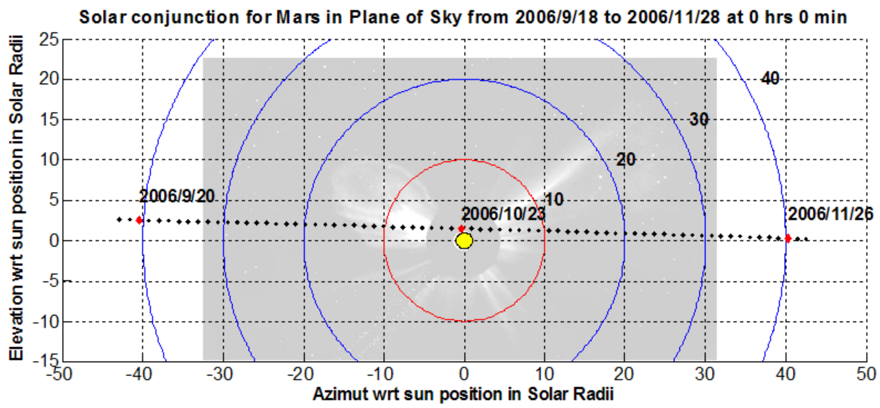

Fig. 2. : Mars Solar Conjunction 2006 as seen from Earth in the plane of sky (solar ecliptic system).

The faint background in Fig. 2 shows a LASCO (Large Angle and Spectrometric Coronagraph) image with a CME and streamer (the LASCO image is roughly adjusted to the plot). This overlay nicely demonstrates some typical structures present in the region of space investigated with coronal radio sounding. The Earth to Mars distance for SCO measurements is approx 2.4 AU.

3.2 Observables

The observables or changes on the carrier signal due to the Solar Corona are

- Group Delay (Ranging),
- Phase Delay (Doppler Shift),
- Faraday Rotation,
- Absorption,
- Amplitude/Phase Scintillation and
- Angular/Spectral Broadening.

They are discussed for example in RD 12 and RD 38.

3.3 Determinable physical quantities of the SCO experiment are:

3.3.1 Total electron content (Ranging)

The number of electrons in a column along the line of sight (LOS) between S/C and G/S can be derived from the delay difference of ranging signals at the 2 downlink frequencies.

The ranging signal is a collection of tone frequencies that are modulated onto the carrier. The tones are separated in frequency such that phase ambiguities of the highest tone frequency (shortest wavelength) can be resolved (AD 01, AD 02).

In this case the frequency of the highest tone, the integration time (width) and the S/N ratio define the accuracy and precision of the S/C topocentric range. For example, a 1° phase uncertainty for a 1 MHz ranging tone results in a position error along the line of sight of ca. 1 m.

The ranging measurement must be conducted at two frequencies in order to separate frequency dependent (plasma effects) from frequency independent (e.g. velocity) effects on the signals.

The total time the ranging signal needs to travel from transmitter to receiver depends on the group velocity. Plasma contributions to the group velocity are frequency dependent (dispersive) and therefore different at S-and X-band. The geometrical free space travel time at the speed of light is equal at both frequencies. This presents the possibility of separating plasma effects from geometrical effects.

Fig. 3 schematically shows the geometrical separation of uplink and downlink due to the movement of the ground station during the time span of the 2 way light time.

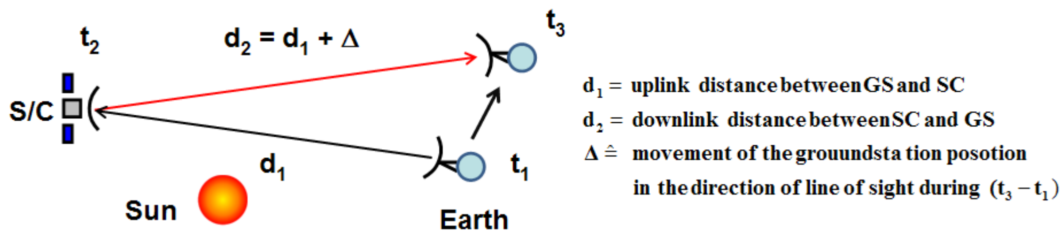

Fig. 3. : Ranging geometry between S/C and G/S. The quantity Δ can be positive or negative.

The group or phase delay time of a signal travelling through a plasma environment is given by [RD 11].

$$T_{gr/ph} \;=\; \int \frac{ds}{v_{gr/ph}} \;=\; \frac{s}{c} \pm \frac{40.31}{c f^2} \int_0^s N_e \, ds = \frac{s}{c} \pm \frac{40.31}{c f^2} TEC \qquad (3.1)$$

The travel time change due to the number of electrons on the path can be expressed as a radio wave or optical path length change s_{Plasma} divided by c. Then s_{Plasma} is defined by

$$\boxed{s_{Plasma} \;=\; \frac{40.31}{f^2} \int_0^s N_e \, ds \;=\; \frac{40.31}{f^2} TEC} \qquad (3.2)$$

The travel distance of the up- and downlink path is

$$\begin{aligned} & S = d_1 + d_2 = 2 d_1 + \Delta \\ & S_{\substack{measured \\ Phase}} = S + S_{Plasma} = d_1 + s_{up\ plasma} + d_2 + s_{down\ plasma} \end{aligned} \qquad (3.3)$$

The plasma contribution on the carrier signal can be expressed by number of electrons in the path per m^2. This total number of electrons is usually counted in hexems (1 hexem = 10^{16} el/m^2). The unit 10-16 el/m^2 was named hexem by Tyler 1977 (RD 09, RD 39) but the origin goes back to a time in the mid 1960s (RD 40). First results from a dual frequency ranging experiment were presented in RD 41.

The plasma path delay difference between an S- and an X- signal is:

$$
\begin{aligned}
\Delta s_{S-X\ Band}\Big|_{\substack{measured\\Phase\\Ranging}} &= s_{\substack{Ranging\\S-Band}} - s_{\substack{Ranging\\X-Band}} = \Delta s_{plasma} \\
&= \left(d_1 + s_{up\ plasma} + d_2 + s_{down\ plasma}\right)\Big|_{S-Band} - \left(d_1 + s_{up\ plasma} + d_2 + s_{down\ plasma}\right)\Big|_{X-Band} \\
&= s_{S\_up\ plasma} - s_{X\_up\ plasma} + s_{S\_down\ plasma} - s_{X\_down\ plasma} \\
&= \Delta s_{up\ plasma} + \Delta s_{down\ plasma}
\end{aligned}
\tag{3.4}
$$

Equation (3.4) assumes that the S-band and X-band paths are equal. This is not absolutely true in a plasma environment, but is a good approximation for a tenuous plasma. Some further details are given in RD 21.

The MEX transponder and RDFU configuration for SCO observations are operated with one uplink at S- or X-band and two downlink frequencies, both coherent to the uplink. For this configuration with a single frequency uplink, the path difference as calculated in (3.4) is reduced to $\Delta s_{plasma} = \Delta s_{down\ plasma}$. Using (3.1) and (3.4) we obtain.

$$
\boxed{\Delta s_{down\ plasma} = 40.31\left(\frac{1}{f_s^2} - \frac{1}{f_x^2}\right) TEC_{down}}
\tag{3.5}
$$

$$
\boxed{\Delta \tau_{down\ plasma} = \frac{40.31}{c}\left(\frac{1}{f_s^2} - \frac{1}{f_x^2}\right) TEC_{down}}
\tag{3.6}
$$

The approximated value 40.31 m^3/s^2 is used in (3.1) and (3.2) for the constant $\frac{1}{2}\frac{e^2}{4\pi^2 m_e \varepsilon_0}$ and TEC_{down} is defined as $\int_{SC}^{GS} N_e\, ds$ in (3.5) and (3.6). Similar equations are presented for example in RD 42.

The S- and X-Band frequencies (f_s , f_x) are known precisely and therefore we obtain from (3.5) a linear relation between the path length change and the TEC along the downlink.

$$
TEC_{down} = c_{Mission}\ \Delta s_{down\ plasma} = c^{\mathrm{I}}_{Mission}\ \Delta\tau
\tag{3.7}
$$

with $c_{Mission} = c^{\mathrm{I}}_{Mission} / c$ and c is the speed of light. The constant $c_{Mission}$ is slightly different for the three S/C VEX, MEX, and ROS, due to slight differences in the S- and X-band carrier frequencies. $\Delta\tau$ is the group delay difference between the S- and X-band ranging codes (see also RD 16).

For Mars Express the nominal S- and X-Band frequencies are 2296.432 MHz, 8420.432 MHz (RD 02) and the relation (3.7) becomes

$$\boxed{TEC_{down\_MEX} = 4.240\ \Delta\tau_{down\ plasma}} \tag{3.8}$$

where TEC is given in hexem and the differential delay time $\Delta\tau$ is given in ns.

The two-way dual-frequency link used on MEX does not allow a determination of TEC for the uplink. Independent values of the up- & downlink TEC requires five different radio links. A possible configuration is to use two signals in different frequency bands for the uplink and three signals in at least two different frequency bands for the downlink. Moreover, all carriers must be modulated with a ranging signal (see also chapter 4.8).

A more detailed description for the analysis of ranging data is given in RD 01, Applicable documents are AD 02 and for the DSN sequential ranging AD 01

3.3.2 Change of TEC (Doppler)

Most deep space missions are able to switch on a second downlink signal in another frequency range, but driven by the same reference oscillator as the usually used downlink signal. This coherent dual-frequency downlink can also be used to study the plasma content along the line of sight. Because of the ambiguity in the measurement of the total phase of a received signal, it is only possible to determine the change in TEC from the beginning of the recording.

The advantage of the carrier signal frequency measurements is the normally higher S/N ratio and the short wavelength with respect to the ranging measurements, thereby yielding a much smaller error bar on the TEC values. The observed differential Doppler frequency shift follows the change in electron content along the line of sight as a function of time (similar to the differential ranging data).

The received signal frequency at the ground station is

$$\begin{aligned} f_{rec} &= f_0 - \frac{v_{rel}}{c}\ f_0 + \frac{40.31}{c}\ \frac{1}{f_0}\ \frac{d}{dt}\int_{SC}^{Earth} N_e\ dy \quad \left(+\ \texttt{other}\right) \\ &\cong f_0 - \frac{v_{rel}}{c}\ f_0 + \frac{40.31}{c}\ \frac{1}{f_0}\ \dot{TEC} \end{aligned} \tag{3.9}$$

All contributions grouped in the word ‘`other`’ are not discussed here. More details are given in RD 19.

$$f_{rec} = k_{X,S}\left(f_{up} + f_{up\_Dop} + \Delta f_{up\_plasma}\right) + f_{down\_Dop} + \Delta f_{down\_plasma} \tag{3.10}$$

The constant $k_{X,S}$ (X for X-band and S for S-band) reflects the coherent frequency muliplicator introduced on the S/C between uplink and downlink and is given by the transponder ratios

$$k_{X_{down}/X_{up}} = \frac{f_{X_{down}}}{f_{X_{up}}} = \frac{880}{749} \qquad\qquad k_{S_{down}/X_{up}} = \frac{f_{S_{down}}}{f_{X_{up}}} = \frac{240}{749} \tag{3.11}$$

The frequency ratio between S- and X-band is

$$k_{S/X} = \frac{f_S}{f_X} = \frac{3}{11} \tag{3.12}$$

Using these constant relations the downlink plasma residual calculated from the **differential Doppler** of the downlink signals is

$$\Delta f_{Plasma} = f_{rec\_S} - \frac{3}{11} f_{rec\_X}$$

(3.13)

$$\Delta f_{Plasma} = \frac{\dot{s}}{c} f_S + \frac{40.31}{c} \frac{1}{f_S} \dot{TEC} - \left(\frac{3}{11} \frac{\dot{s}}{c} f_X + \frac{40.31}{c} \frac{f_S}{f_x^2} \dot{TEC} \right)$$

$$\boxed{\Delta f_{Plasma} = \frac{40.31}{c} f_S \left(\frac{1}{f_S^2} - \frac{1}{f_X^2} \right) \dot{TEC}} \tag{3.14}$$

$$\boxed{\dot{TEC} \cong \frac{\Delta TEC}{\Delta t} = \frac{c}{40.31} f_S^{-1} \left(\frac{1}{f_S^2} - \frac{1}{f_X^2} \right)^{-1} \Delta f_{Plasma}} \tag{3.15}$$

All quantities in (3.15) except the time derivative of the TEC are known. Integration of this equation vs. time yields TEC(t) from the beginning of the measurement:

$$\boxed{TEC = \left[\frac{40.31}{c} f_S \left(\frac{1}{f_S^2} - \frac{1}{f_X^2} \right) \right]^{-1} \int_{t_0}^{t} \Delta f_{Plasma} \, dt + TEC_0} \tag{3.16}$$

The value TEC_0 can only be achieved by a two frequency band ranging measurement.

A detailed description for the analysis of IFMS Doppler data is given in RD 02.

3.4 Coronal Electron density

One of the first studies of the electron density distribution of the solar corona was done by Baumbach (RD 07) , who used the available coronal brightness data. The fit to the brightness was transformed via an Abel Integral to the electron density distribution with the following radial dependence.

$$N(r) = 10^8 \left(\frac{0.036}{r^{1.5}} + \frac{1.55}{r^6} + \frac{2.99}{r^{16}} \right) \tag{3.17}$$

Allen (RD 08) improved the model by separating the source of the coronal brightness into two parts:

- sunlight scattered on electrons
- Fraunhofer lines emitted from atoms.

The equation (3.17) was further modified to include latitudinal effects. For example, Tyler et al. (RD 09) and Pätzold et al (RD 16) have used the expression (3.18).

$$F(\phi) = \sqrt{A^2 \cos^2 \phi + \sin^2 \phi} \tag{3.18}$$

Muhleman (RD 10) used a Gaussian latitudinal variation and obtained the following parametric fit to the Viking coronal sounding data.

$$N_e = \frac{1.32 \cdot 10^6}{\left(r/R_\odot \right)^{2.7}} e^{-\left(\frac{\phi}{\phi_S} \right)^2} + \frac{2.3 \cdot 10^5}{\left(r/R_\odot \right)^{2.04 \pm 0.02}} \tag{3.19}$$

The solar latitude is represented by φ and for the Viking experiment the best fit was received with $\varphi_S = 8^\circ \pm 3^\circ$. The distance of the line of sight to the sun centre is r and $R_\odot$ is the sun radius.

Bird et al. (RD 15) adapted the following equation (3.20) to the special geometry applicable to the Ulysses solar conjunction in 1991:

$$\boxed{N(r,\phi) = \left[N_A \left(\frac{R_\odot}{r} \right)^6 + N_B \left(\frac{R_\odot}{r} \right)^\alpha \right] F(\phi)} \tag{3.20}$$

It was found that the two terms in $F(\phi)$ and the term in r^{-6} were negligible for the ranging dataset recorded during the 1991 Ulysses conjunction. This simplified the formula and only the term with $r^{-\alpha}$ remained. The integration of (3.20) along the downlink ray path from Ulysses to earth yields (RD 15)

$$TEC = K(\alpha)\, N_B\, R_\odot \left(\frac{R_\odot}{r} \right)^{\alpha - 1} \tag{3.21}$$

with

$$K(\alpha) = \int_{-\pi/2}^{\pi/2} \cos^{\alpha - 2} \phi \, d\phi = \sqrt{\pi} \left[\Gamma\left(\frac{\alpha - 1}{2} \right) \Big/ \Gamma\left(\frac{\alpha}{2} \right) \right] \tag{3.22}$$

Bird (RD 11) presents a summary of SCO measurements performed from the beginning until approx. 1981. Fig. 4 shows on the left a contour plot of the TEC in the ecliptic plane (left subpanel) and in a polar plane (right). The plot is based on the density model derived from Tyler et al. (RD 09). Some models of the latitude dependence are shown on the right panel of Fig. 4 (RD 20)

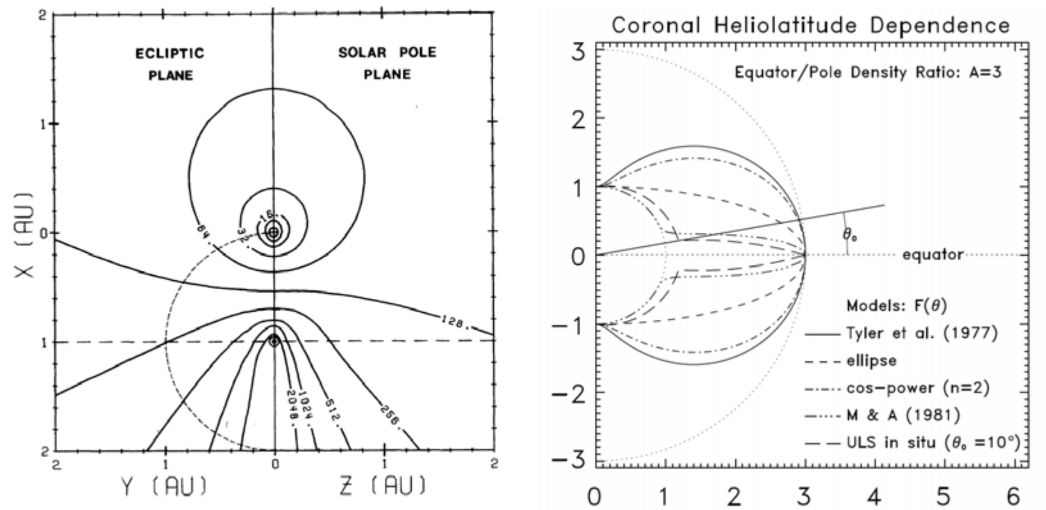

Fig. 4. : Left panel: *TEC* in the x-y plane (solar ecliptic, left subpanel)) and in the x-z plane (solar pole, right subpanel) from RD 11. The lines of constant TEC are given in hexem = 10^{16} el m^{-2}. The plot is based on the model taken from RD 09. Right panel: Some different models for the heliospheric latitude dependency as shown in RD 20.

Step by step procedure for the calculation of α and N_B:

- Use equation (3.8) to obtain TEC(t) for each tracking pass during the solar conjunction.
- Calculate the mean value of TEC for every pass
- Apply a least-squares algorithm to fit the observed TEC values to (3.21)

$$TEC = N_B\, R_\odot \left(\frac{R_\odot}{R} \right)^{\alpha - 1}$$ in order to derive α and N_B

The best fit density is defined by (3.20) and can be used for further interpretation

A correction for ranging observations near solar conjunction, based on a formula by Anderson (RD 13), is described in detail in RD 14.

3.5 Coronal Mass Ejections (CMEs)

Coronal Mass Ejections are massive eruptions of plasma from the Sun. If this plasma disturbance travels through the line of sight between Earth and S/C during a two-way tracking session (Fig. 5), both the uplink and downlink signals are modulated by the change in the TEC. In a coherent two-way link configuration, each part of the moving CME that crosses the radio link is sounded once in the uplink and once in the downlink such that these events are recorded twice in the received data. The CME signature modulated near time t_0 (Fig. 5) on the signal will be seen in the received data at the G/S on the downlink at t_1 and a second time at t_3 after the signature on the uplink travels to the S/C and then coherently back to the G/S. The region of the event marked with time t_0 will be discussed further in more detail.

A description of an algorithm separating the plasma effects on the up- and downlink signal is given in chapter 3.6 and 4.8.

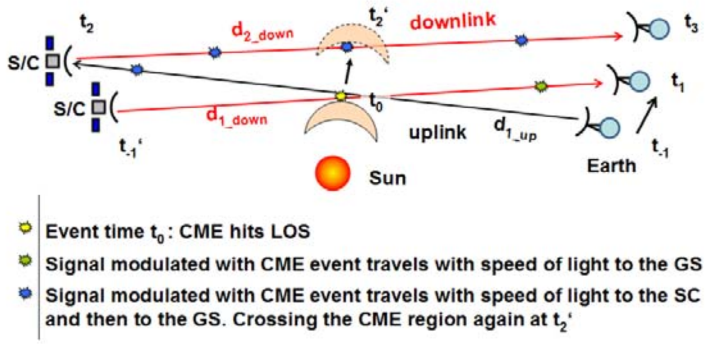

Fig. 5. : Propagation of the CME and the modulated radio signal vs. time. The modulation event at t_0 indicated due to the yellow mark travels along the downlink path indicated by the green mark towards the ground station and indicated by the blue markings upwards to the S/C and then back to the ground station. On that downlink path the CME is sounded again but on a different CME region. This second event is indicated in the drawing with the time t_2'. The details around time t_0 are discussed further.

The following two examples are chosen in order to understand the geometry of the up- and downlink paths. Using this knowledge, it is explained how the TEC signature in the data sets can be used to calculate the approximate velocity of the CME.

The easiest example for the geometry between S/C and G/S is given by the special case shown in Fig. 6. It is assumed that S/C and G/S have equal velocities and directions. The plot shows that for this special case the up- and downlink signal positions are not separated for any time t. As a result there is no possibility to calculate a CME velocity but in this special case it is possible to get the point in space and time where the modulation occurred

A more detailed description follows below.

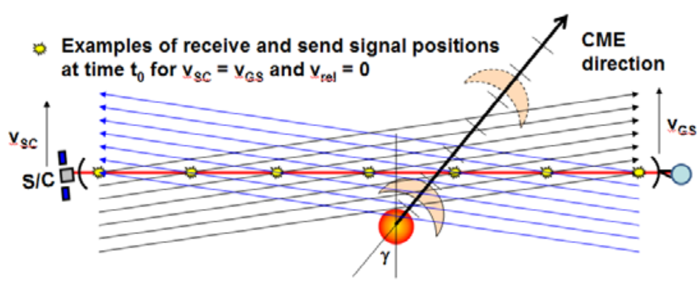

Fig. 6. : Schematic for the position of the signals in space at a defined time t_0 for the up- and downlink. The velocities of the ground station and spacecraft are similar and parallel. The red line indicates all microwave signal positions that were sent in the past from the S/C and the G/S and will arrive in the future at the G/S and the S/C. The yellow markings indicate the positions of the signals that will be received in future. Along the black lines the position is given for the downlink and along the blue lines for the uplink.

In Fig. 5 the position of the event t_0 in space time is approximated due to the cross of the black uplink- d_{1_up} with the red downlink-line d_{1_down} and the location of the event where the CME touches the signal. For this special example is “exactly” defined due to the cross at t_0. The signal paths and the S/C- and G/S locations for the event at t_0 are given by the receiving times t_1 and t_3.

The cross point derived from the locations of the G/S at the receiving times defines the position where the CME has hit the microwave link (as shown in Fig. 6). Assuming a radial velocity of the CME from the sun to this point, the line sun centre – cross point shows the direction of the travelling plasma.

In this first example it is not possible to get a velocity value of the CME because there is no difference in the location of the modulation on the uplink and the downlink signal as mentioned before.

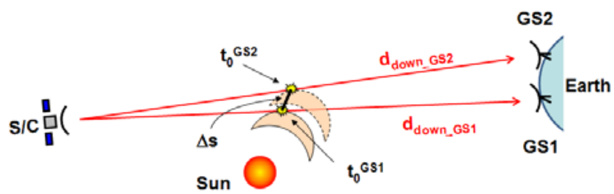

Fig. 7. : Geometry for the velocity determination of a CME with 2 ground stations

In general it is possible to observe with a 2nd ground station at the same time. With the 2nd dataset the velocity of the CME can be calculated by using the time difference of the CME features on the two different downlink paths (RD 06, RD 17) and the distance between the events in time and space. The direction for the CME has to be contributed by another experiment. Fig. 7 shows the geometry for this observation with a 2nd ground station.

The 2nd example (Fig. 8) is still simple, because the relative velocity of the G/S is zero with respect to the sun but the example shows nively the split of the locations of the up- and downlink signal paths for a defined time t_0.

The locations of the signals that were sent in the past but haven't reached the receiving units on the S/C and G/S side are travelling along the black lines (downlink) and along the blue lines (uplink). The positions of the shown signal locations are separated by Δt=LT/7 on the example paths and are marked blue or yellow. A theoretical connection of the yellow uplink marker points would reflect the location of the continuous signal that will be received at the S/C in the future and similar, doing the same with the blue markers, it would show the continuous signal positions that will be received in the ground station in the future for this time t_0. The plot makes obvious that the modulation of the signals due to the crossing CME on the up and downlink takes place at different times and locations.

This behaviour that the up and downlink positions are separated can be generalized as long as there is a relative velocity between S/C and G/S. Therefore this 2nd example reflects the general case with nonlinear changing velocity vectors. For the general case the only difference will be, that the signal locations for every timestamp t_0 will be a little bit more twisted.

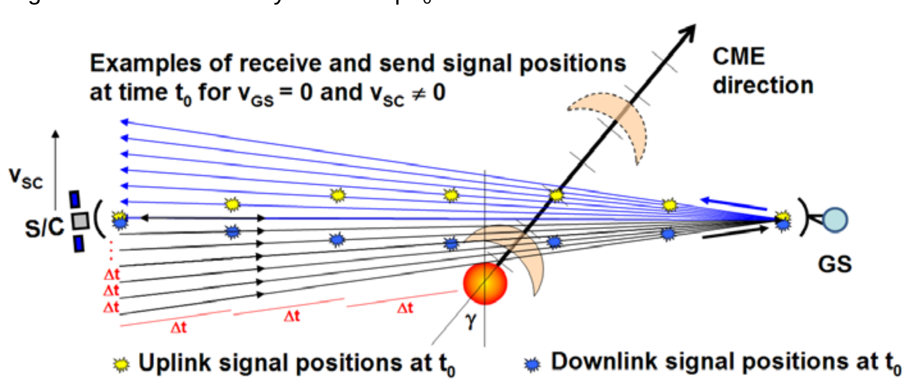

Fig. 8. : The 2nd example for the location of the uplink and downlink signals at time t_0. The shown example reflects also the normal case with nonlinear velocity changes between G/S and S/C. The

marked example radio signal positions (yellow and blue dots) will only be a bit more twisted in the 3d space. This example shows explicit that the uplink and downlink modulation does not take place at the same position and due to that also not at the same time as in the 1^{st} example in Fig. 6.

The conclusion of the short exercise is, that the up- and downlink signals have a separation in space and therefore features in the electron content of the CME are separated in time on the received up- and downlink signal. The structure of the whole electron content is seen (received) in the microwave phase shift twice. The two modulated plasma shifts are from different times and locations on the uplink compared to the downlink.

Similar to the conclusion for the 2 station observation it is possible to calculate the CME velocity for cases where the direction of the CME is detected by other instruments.

Fig. 9 is based on the previous discussion and shows the geometry for the CME event that modulates the downlink signal at $t_{0\ down}$ and the uplink signal at $t_{0\ up}$. The paths and with that all points P and the related times t on the paths in the plot are defined by the received times t_{1r} and t_{3r}. The received times of the events allow a reconstruction of the geometry.

For further considerations it is assumed that the CME velocity vector penetrates in a radial direction from the sun and that the direction is known by additional information. In case the direction is not known an approximated velocity can be calculated for the signal path tangential point. This enables to allocate the points $P(t_{0\ up})$ and $P(t_{0\ down})$.

With this information the CME crossing event on the up- and downlink can be reconstructed as shown in Fig. 9. All times and locations are known and the velocity can be calculated using equation (3.23).

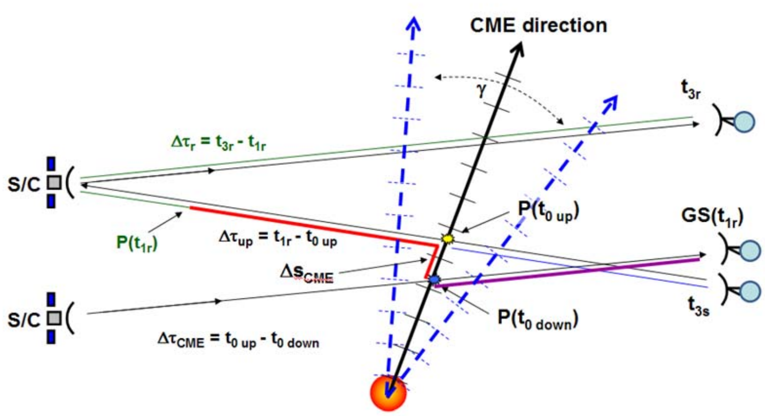

Fig. 9. : Location of the CME direction in Space and Time for the general case of different velocity vectors for S/C and G/S.

$$v_{CME} = \frac{\Delta s_{CME}}{\Delta \tau_{CME}} = \frac{P_r(t_{0\ up}) - P_r(t_{0\ down})}{t_{0\ up} - t_{0\ down}} \tag{3.23}$$

$P_r(t)$ = radial distance from the sun at time t. Assumed is a “constant or not changing” shape of the electron number in the region of the up and downlink signal.

Fig. 9 shows the radial distances of the paths that are used in equation (3.23). It might be possible to get a higher degree of correlation on the residual phase shifts between up and downlink by differentiating between fast and slow TEC changes. The low frequency changes will have a higher correlation and therefore a smaller velocity uncertainty.

The fast TEC changes allow analyzing finer structures in the corona like small waves or boundaries but it has to be taken into account that the location of the changes is local or on parts of the signal path only and the correlation is maybe not unique.

A split of the received dataset in parts with features might give a velocity series over time.

In addition to the separation of the up- and downlink path the different bending of the up- and down-link frequencies has to be analyzed carefully. The difference of the bending on X and S band signals contributes to the offset between up- and downlink signal paths Δs_{CME}.

The usual configuration for SCO observations is X_{up} and coherent X_{down}- & S_{down}. This configuration enables a double check on the derived CME velocity which should be equal for the $X_{up} – X_{down}$ and $X_{up} – S_{down}$ analysis.

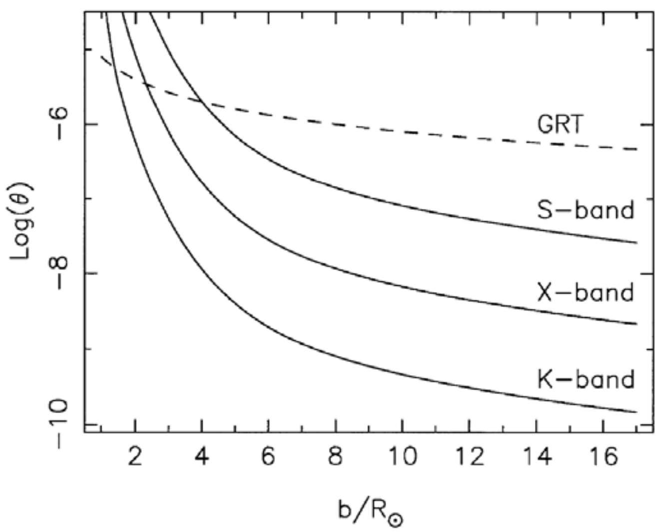

Fig. 10. : Radio signal deflection due to the solar corona on the S- X- and K-Band as shown in RD 21 and RD 22

The knowledge of the TEC on the downlink path (derived by the differential ranging) theoretically enables to approximate the bending difference and the ray path distance at the downlink between X- and S-Band TEC features of the less noisy Doppler data. Fig. 10 shows the bending of a radio signal for the 3 frequency bands S, X and K as a function of the rayparameter (tangential distance of the signal path from the sun) in solar radii.

For example, an S- and X-band signal at 5 radii will have a bending difference of approx. 10^{-6} deg. This angular difference of the bending results in a distance between the rays of approx. 150 km (for a G/S position at 1 AU and an infinity position of the S/C). Applying a normal speed for the CME of 400 km/s the time difference on the downlink is approx. 0.25 s. This difference might be detectable in the downlink band pass filtered TEC residuals by a correlation on a data set of S- and X-Band data points (see also 4.8).

In theory the following procedure can be used:

- Calculate the Doppler residuals for the received S- and X-Band frequencies (received values minus calculated values).
- Filter the S and X-Band residuals as described in 4.8 (usage of undisturbed features)
- Calculate the received time difference of similar features in X-and S-Band in a correlation analysis

3.6 Separation of up- and downlink frequency shifts due to the plasma contribution on the recorded radio signal

A method that allows separating the plasma frequency shifts on the uplink and downlink path is well described in RD 18 and similar described below.

As mentioned before the method assumes that the S- X-Band propagates along the same downlink path and that the modulation occurs at the same time. This is not absolutely true because of the different bending the paths at closest approach are separated and the moving plasma will create the events on the signal at slightly different times too. In case a difference in the modulation of the downlink bands is detected It might be possible to find an iterative process to take this into account but it is not further investigated here.

With equation (3.15) and the constant ratios between up- and downlink frequencies as given in (3.24)

$$f_S^2\left(\frac{1}{f_S^2}-\frac{1}{f_X^2}\right)=\frac{112}{121} \tag{3.24}$$

we get for the S-Band plasma downlink contribution

$$\dot{TEC}\cong\frac{\Delta TEC}{\Delta t} = \frac{c}{40.31}\, f_S^{-1}\left(\frac{1}{f_S^2}-\frac{1}{f_X^2}\right)^{-1}\Delta f_{Plasma}$$

$$\begin{aligned}\Delta f_{Plama,\,down,\,S} &= \frac{40.31}{c}\,\frac{1}{f_S}\,\dot{I} = \frac{40.31}{c}\,\frac{1}{f_S}\,\frac{\Delta I}{\Delta t}\\ &= \frac{40.31}{c}\,\frac{1}{f_S}\,\frac{c}{40.31}\,\frac{1}{f_S}\left(\frac{1}{f_S^2}-\frac{1}{f_X^2}\right)^{-1}\Delta f_{Plasma}\\ &= \frac{121}{112}\,\Delta f_{Plasma}\\ &= \frac{121}{112}\left(f_{rec\ S}-\frac{3}{11}\ f_{rec\ X}\right)\end{aligned} \tag{3.25}$$

And similar for the X-Band downlink contribution

$$\begin{aligned}\Delta f_{Plama,\,down,\,X} &= \frac{40.31}{c}\,\frac{1}{f_X}\,\dot{I} = \frac{40.31}{c}\,\frac{1}{f_X}\,\frac{\Delta I}{\Delta t}\\ &= \frac{40.31}{c}\,\frac{f_S}{f_X}\,\frac{c}{40.31}\,\frac{1}{f_S^2}\left(\frac{1}{f_S^2}-\frac{1}{f_X^2}\right)^{-1}\Delta f_{Plasma}\\ &= \frac{3}{11}\,\frac{121}{112}\,\Delta f_{Plasma}\\ &= \frac{3}{11}\,\frac{121}{112}\left(f_{rec\ S}-\frac{3}{11}\ f_{rec\ X}\right)\end{aligned} \tag{3.26}$$

Finally the X-Band uplink plasma contribution on the signal can be calculated from equation (3.9) after a correction for the movements of the S/C and G/S and further calibrations see e.g. RD 02 and chapter 4.8.

$$\begin{aligned}\Delta f_{Plasma,\,up,\,X} &= \frac{749}{880}\left(\Delta f_{Plasma,\,X} - \Delta f_{Plasma,\,down,\,X}\right)\\ &= \frac{40.31}{c}\frac{1}{f_{up\ X}}\dot{I}_{up}\end{aligned} \tag{3.27}$$

With the equations (3.25) - (3.27) 3 datasets are available but the 2 downlink datasets do not have additional information with respect to each other. It has to be mentioned also that the uplink value gets a small error due to the downlinks path separation and that is not taken into account in the equations above.

The up- and downlink data still has a strong correlation on the solar corona electron content because the separation in time and location of the paths is small with respect to the change of the features in time and with location. The data is used for the feature velocity calculation as described in 3.5.

3.7 Further studies on solar corona data

3.7.1 Scintillation

Scintillation effects are observed while a radio source is located close to the sun with respect of the receiving antenna. The variation of the plasma density inside of the Fresnel Zone and multipath effects are causing amplitude variations in the received signal strength. Because the effect occurs on the path between source and receiver the effect is named Interplanetary Scintillation (IPS).

Many papers are published on scintillation effects due to solar corona measurements. Some reference documents are RD 26, RD 27, RD 28.

3.7.2 Spectral Analysis

The analysis of frequency fluctuation spectra of differential Doppler data has revealed a quasi periodic component around 4 mHz in some datasets. References are RD 24, RD 25 and RD 29.

3.7.3 Ephemerides Calculation

The extension of the solar corona is the solar wind. There is a direct connection between electron density and solar wind and investigations are done to use the solar corona content measurements in order to achieve more precise values for the solar wind and to adapt this solar wind force on small bodies' ephemerides predictions RD 23.

4 Description of a SCO PSA data set

The archive structure and types of data sets are explained in the following subsections. The different levels of data sets are well described in existing documentation available in the archive. Hence, only a short summary and references are presented here.

4.1 MEX archive access

The MEX archive is available on the web at

http://www.rssd.esa.int/index.php?project=PSA&page=mex

and the ftp site at

ftp://psa.esac.esa.int/pub/mirror/MARS-EXPRESS/

On the main web page a link is shown that is indicated as “Advanced search” (currently a green button).

A click on this button starts a Java based popup window that allows a query search (advanced search) by enabling or choosing menu items. Make sure that your browser has Java enabled and allows showing popups from the ESA webpage www.rssd.esa.int.

After the click a popup window appears and shows the following menu structure.

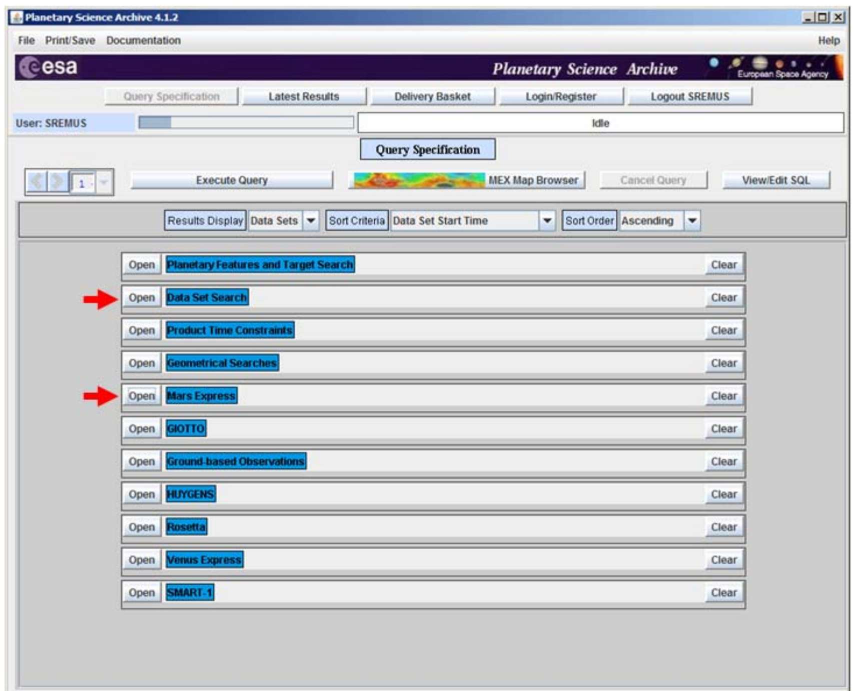

Fig. 11. : ESA archive main search page. The red arrows indicate the menus that are needed for the MEX solar corona data sets search

After clicking on “Data Set Search” and “Mars Express”, one may browse for SCO data in the MEX archive with the settings shown below.

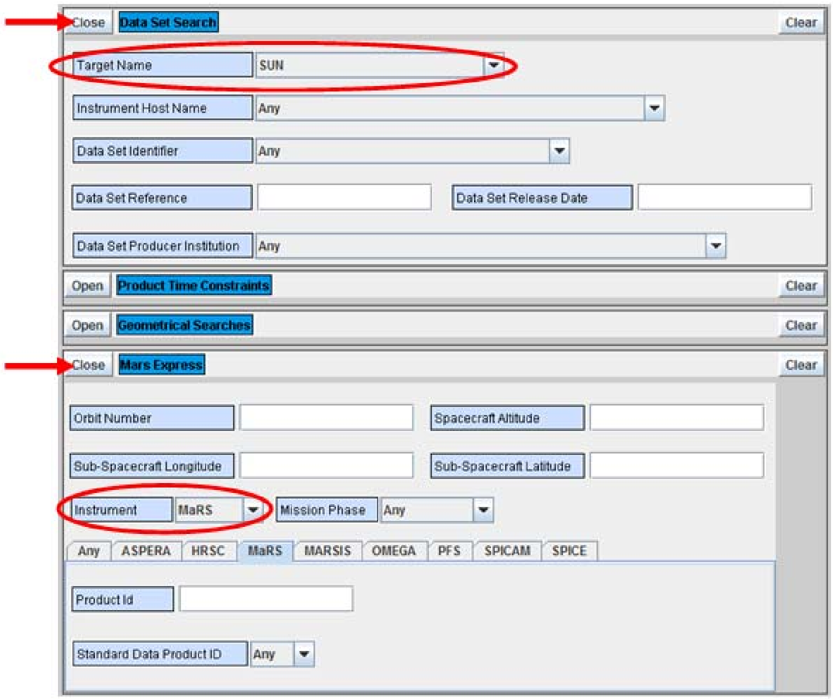

Fig. 12. : Settings for the MEX SCO data sets search: 1 - Data set search/Target Name/Sun, 2 - Mars Express/Instrument/MaRS.

The “Execute Query” – button (see Fig. 13) starts the search and shows a list of the available data sets as shown in Fig. 14. The header shows the number of MaRS data sets with SCO data that are currently in the PSA archive.

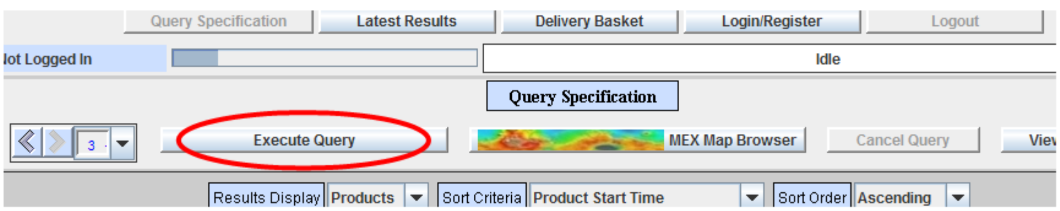

Fig. 13. : Execute Query button

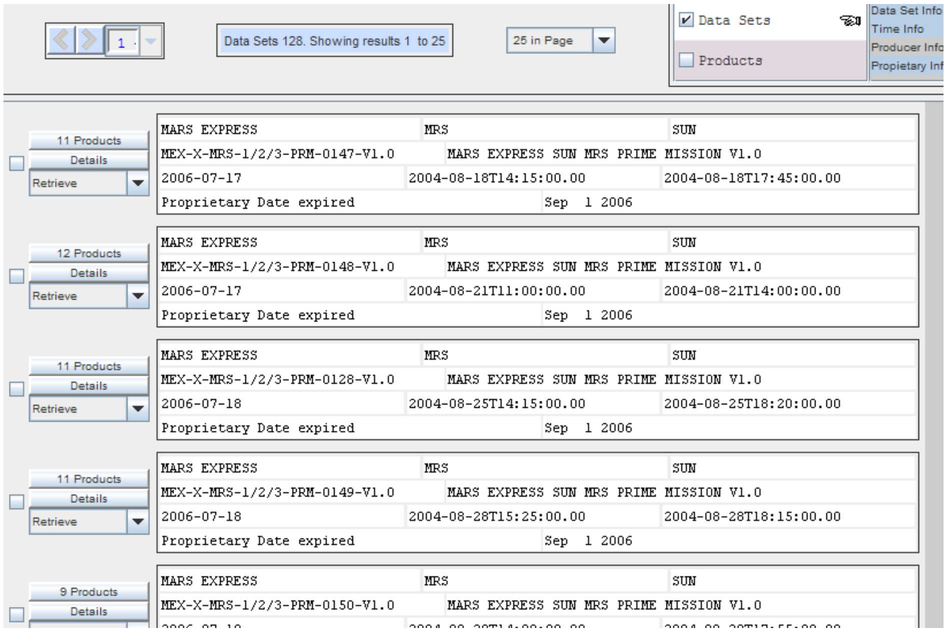

Fig. 14. : MEX SCO query result: List of observations (datasets)

The result of the query is a list of data sets with a possibility of selecting an individual data set for download and detailed analysis. A list of the folder names is shown in Appendix A. A description of the file name convention is available in RD 04 and in the **dataset.cat** file. The dataset.cat file can be displayed as follows: On the advanced search data sets result window click on “Details” (on the left side beside each data set) and then on “DATASET.CAT”.

All folders have the generic structure: XXX-Y-ZZZ-U-VVV-NNNN-WWW

The first folder in the list is: MEX-**X**-MRS-1-2-3-PRM-0147-V1.0

The first entry (3 letters) in the folder name is MEX. The second entry of the folder name (Y) gives the target ID of the observations. No explicit target ID is assigned to the SCO observations and therefore the general character X is used. This means all SCO data sets have the X in the folder name, but the X does not necessarily mean that the data are SCO. For example the folder MEX-X-MRS-1-2-3-EXT1-0888-V1.0 contains Phobos gravity data.

Some links to the MEX archive **ftp pages** are shown below**:**

The Archive Generation, Validation and Transfer Plan for the radio science experiments on MEX, Rosetta and VEX shows structures, data types and levels that are available in the PSA. The document is available at:

ftp://psa.esac.esa.int/pub/mirror/MARS-EXPRESS/MRS/MEX-M-MRS-1-2-3-CR1-0009-V1.0/DOCUMENT/MRS_DOC/MEX-MRS-IGM-IS-3019.PDF

The **MEX Radio Science data** is available on ftp at:

ftp://psa.esac.esa.int/pub/mirror/MARS-EXPRESS/MRS/

Some MaRS instrument information is summarized in the file inst.cat (for example the ground station locations):

ftp://psa.esac.esa.int/pub/mirror/MARS-EXPRESS/MRS/MEX-M-MRS-1-2-3-CR1-0009-V1.0/CATALOG/INST.CAT

4.2 ROS archive access

The ROS archive is available on the web at

http://www.rssd.esa.int/index.php?project=PSA&page=rosetta

and the ftp site at

ftp://psa.esac.esa.int/pub/mirror/INTERNATIONAL-ROSETTA-MISSION/

On the main web page a link is shown that is indicated as “Advanced search” (currently a green button).

A click on this button starts a Java based popup window that allows a query search (advanced search) by enabling or choosing menu points. Make sure that your browser has Java enabled and allows showing popups from the ESA webpage www.rssd.esa.int.

A popup window appears with the menu as shown in Fig. 15. The settings for ROS are slightly different than those used for the MEX mission.

The SCO data list as shown in Fig. 18 is the result of the settings as shown in Fig. 15 - Fig. 17.

Note: Before hitting the “execute query” button, be sure to set “data sets” in the field for “Results display”. Otherwise, you get a list of ALL products (more than 6000).

Fig. 15. : ESA archive main search page. The red arrow indicates the tab that is needed for the ROS solar corona datasets search

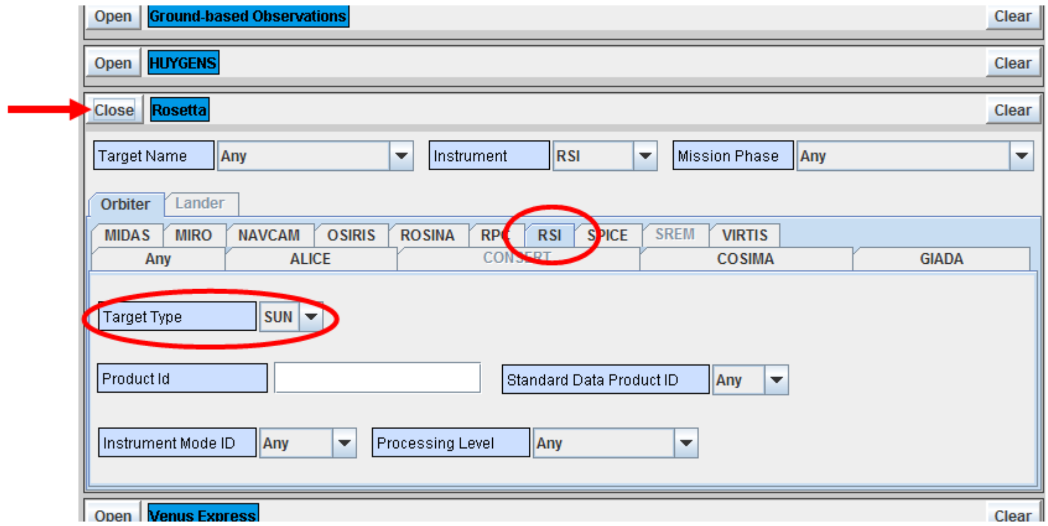

Fig. 16. : Settings for the ROS SCO datasets search. Click on “RSI” and select then the Target Type “Sun”.

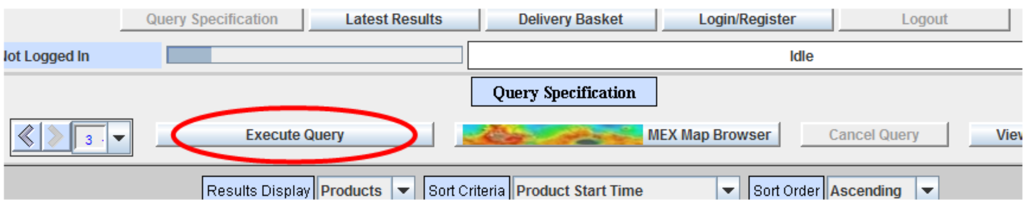

Fig. 17. Execute Query button.

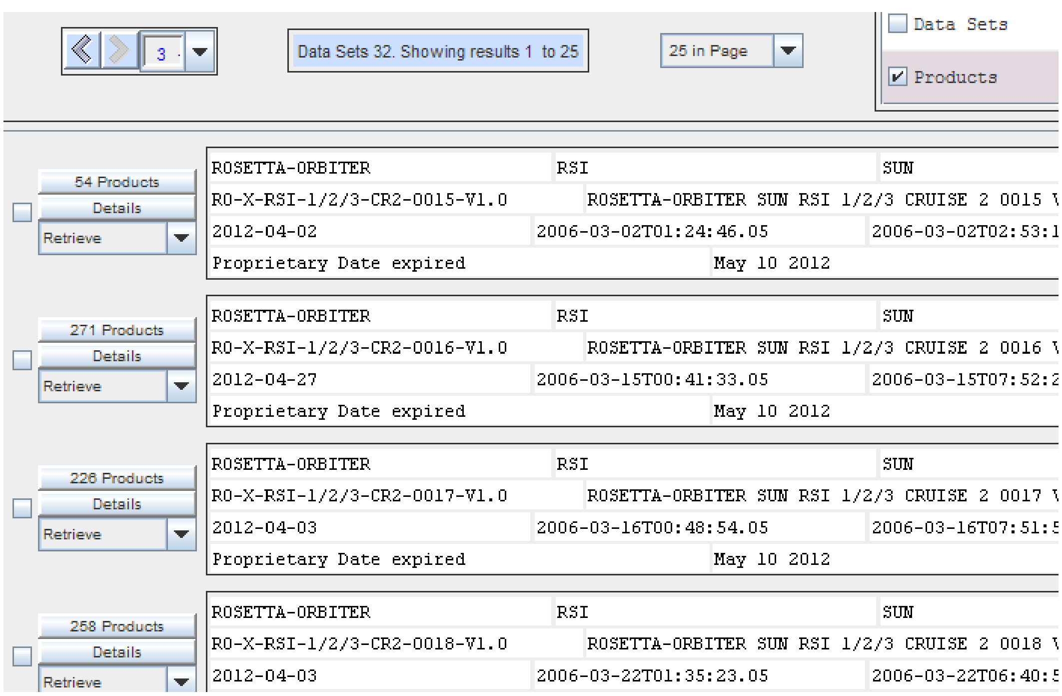

Fig. 18. ROS SCO query result: List of observations (data sets)

The result of the query is a list of data sets with a possibility of individual data set selection for the download. A list of the currently available folder names that have SCO data is shown in Appendix A. A description of the file name convention is available in RD 04 and in the **dataset.cat** file. The dataset.cat file can be displayed as follows: On the advanced search data sets result window click on “Details” (on the left side beside each set) and then on “DATASET.CAT”.

Some links to the ROS archive **ftp pages** are shown below**:**

ftp://psa.esac.esa.int/pub/mirror/INTERNATIONAL-ROSETTA-MISSION/RSI/

Some RSI instrument information is summarized in the file inst.cat (for example the ground station locations):

ftp://psa.esac.esa.int/pub/mirror/INTERNATIONAL-ROSETTA-MISSION/RSI/RO-X-RSI-1-2-3-CVP2-0011-V1.0/CATALOG/INST.CAT

4.3 NASA PDS archive

The link to the MEX radio science data on the PDS is available at

http://pds-geosciences.wustl.edu/missions/mars_express/mars.htm.

The MEX data is partitioned by mission times which are the prime mission and extended missions 1 and 2. In order to know which dataset includes SCO data it is useful to review the most recent aareadme.txt file. To view this file, one must first click on the page called “raw data extended misson 2” and then on the last data file, presently called “mexmrs_3545”.The file lists all radio science datasets and shows the observation type in the description column. SCO datasets are identified by the keyword “Solar Conjunction”.

MEXMRS_0139	2004-08-11	2004-08-11	Global Gravity
MEXMRS_0142	2004-08-14	2004-08-14	Occultation
MEXMRS_0145	2004-08-15	2004-08-15	Global Gravity
MEXMRS_0146	2004-08-15	2004-08-15	Global Gravity
MEXMRS_0147	2004-08-18	2004-08-18	Solar Conjunction
MEXMRS_0148	2004-08-21	2004-08-21	Solar Conjunction
MEXMRS_0149	2004-08-28	2004-08-28	Solar Conjunction
MEXMRS_0150	2004-08-29	2004-08-29	Solar Conjunction

Fig. 19. Part of the aareadme.txt file is shown here as an example. The red circle identifies an SCO data set by the name Solar Conjunction and relates this to the filename of the stored data set. Tthe PDS MEX MaRS web page for the nominal mission lists a directory with the name MEXMRS_0147, which contains a SCO data set.

4.4 Description of the data levels

The archive contains level 1a, 1b and level 2 data. Observations executed with the ESA NNO ground-station normally have files for these 3 levels. The structure of level 1a, 1b, and level 2 data in the PSA is shown in Fig. 20 (left panel).

DSN data do not have a level 1b, but rather only level 1a (Fig. 20, right panel). A second difference in the structure of the DSN data with respect to the NNO data is the OL (open loop) data set in the RSR folder. The DSN level 2 data, shown in the example in Fig. 20, is processed from the level 1a open loop recordings.

The NNO IFMS Level 1a and 1b data consist of

- AG1 and AG2 = amplitude data
- DP1 and DP2 = Doppler data
- RNG = ranging data.

The values of the files AG1 and AG2 are received by the two IFMS receivers, but they might have had different settings in the receiving chain (for example different sample rate or loop bandwidth). The same applies to DP1 and DP2. It should also be noted that the files AG1 and DP1 are not necessarily from the same IFMS

The DSN Level 1a data consists of closed loop (CL) and open loop (OL) data. The CL data is available in the ODF and TNF format, which are described in detail in AD 04 and AD 03. Both file types are saved in a binary format. The TNF format is used for new missions and will replace the ODF files in future missions. For MEX both files are still created but the ODF data is extracted from the TNF file. The TNF data are processed (averaged) and then written to the ODF file. It is recommended to use the TNF files for analysis in case software for reading ODF files is not available. Analysis of data from older missions requires a tool to read ODF files.

DSN OL data sets stored in the level 1a folders represent voltage samples of the incoming signal. The open loop data can be used to reconstruct the signal at times when scintillation or multipathing affects the signal and the CL data are corrupted. Also weak signals that are below a needed threshold level inside of the receiver PLL can be recorded and therefore analyzed further. Another advantage of the OL data is the possibility to adapt filter bandwidths for minimizing the noise in further processing steps. The format structure of the ODF data file (*.dat) is explained in the label file (*.lbl), which is available in the same directory as the data file.

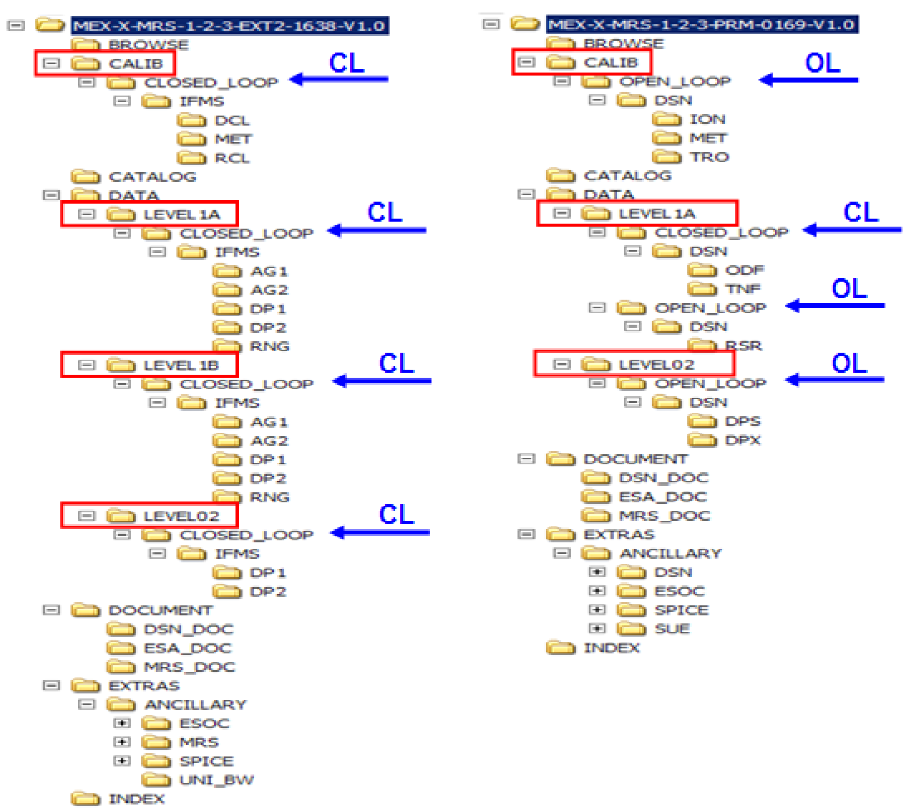

Fig. 20. Screenshot showing parts of the level 1 and 2 SCO dataset structure of the PSA. Left panel

reflects the data structure for an observation with an ESTRACK station and the right panel for a DSN pass. The difference in the settings of the receiving stations causes the difference in the level 1 and 2 data structure.

The next two screenshots (Fig. 21 and Fig. 22) show the data structure of the level 1a and 1b files as generated by the ESTRACK DP1 ASCII CL system. The differences between the data files are obvious, as seen in a comparison of the number of columns. Specifically:

- 1st : the level 1b data file has no header,
- 2nd : level 1b has no characters in the data columns, and
- 3rd : there are two time formats added in columns 3 and 4.

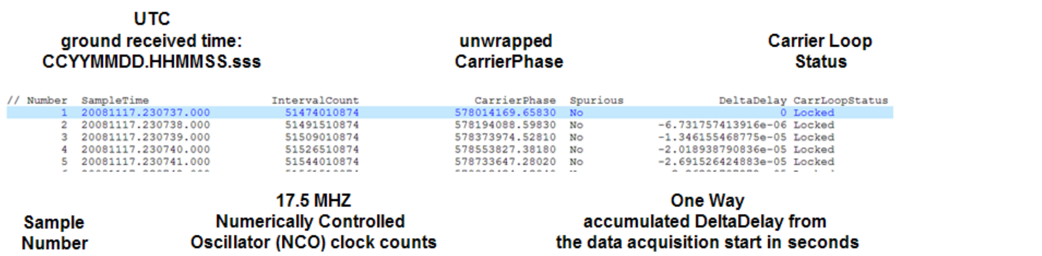

Fig. 21. : Level 1a data with a brief column overview. Data descriptions details are given in AD 05.

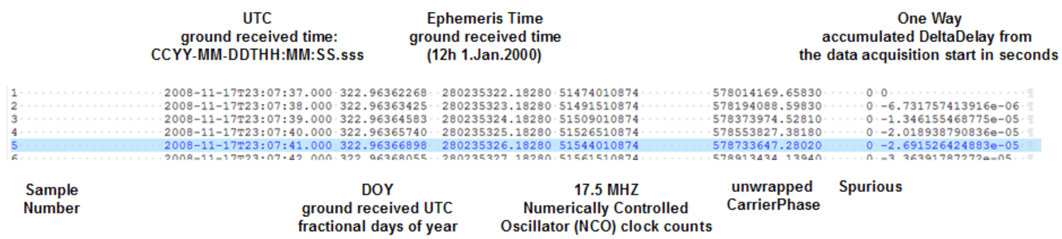

Fig. 22. : Level 1b data with a brief column description. For details see AD 05

The transformation from level 1 to level 2 files includes some data processing and calibration.

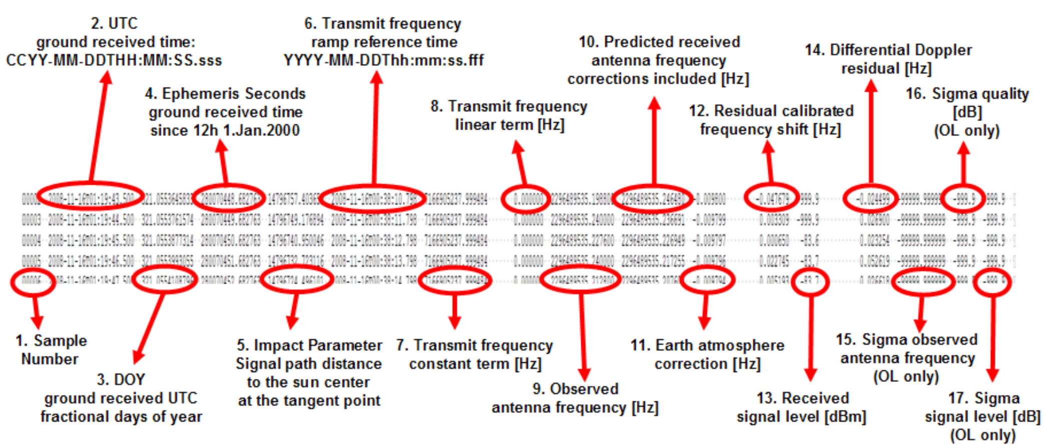

Fig. 23. : Level 2 DP1 data file content description. For more details go to the corresponding label

file.

Example plots generated from three level 2 data sets are shown in Fig. 24 - Fig. 26. The differential Doppler (Fig. 24) contains the change in TEC information along the downlink and can be used for further analysis. The residual calibrated frequency shift (Fig. 25) still has a nonzero offset and drift, in contrast to the differential Doppler. Because of this offset and drift the residuals do not reflect the true change in TEC at this stage of the processing.

The signal level plot (Fig. 26) reflects the resolution of the AGC data. Due to the almost constant power level and the small noise (+/- 0.2 dB), the quantization into 0.1 dB steps is obvious in the high-resolution plot. The signal level shown here excludes the amplification internal to the receiving system and is thus not the absolute received power level at the antenna.

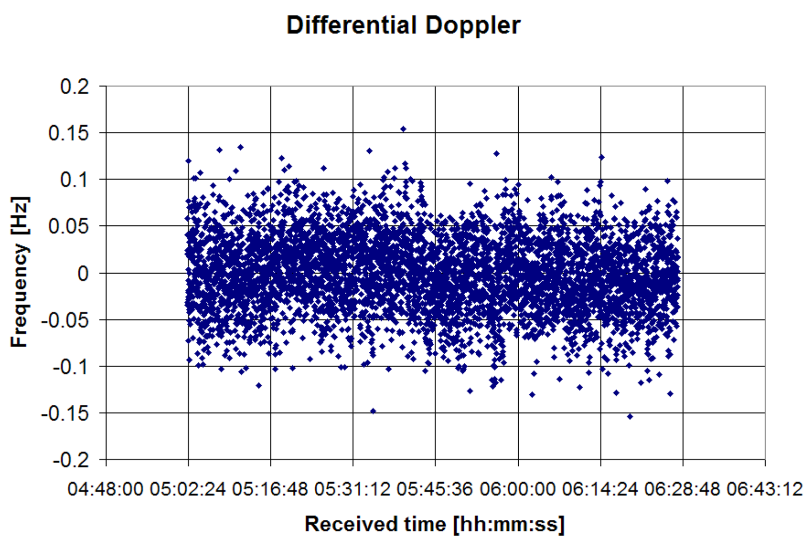

Fig. 24. Level 2 differential Doppler residuals (MEX-X-MRS-1-2-3-EXT2-1623-V1.0\...\DP2\M32ICL2L02_D2X_083120502_00.TAB)

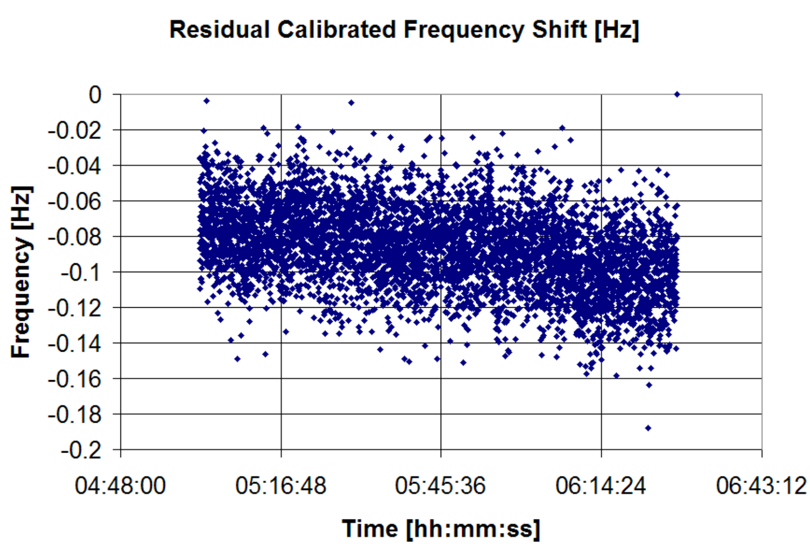

Fig. 25. Level 2 residual calibrated frequency shift (MEX-X-MRS-1-2-3-EXT2-1623-V1.0\...\DP2\M32ICL2L02_D2X_083120502_00.TAB)

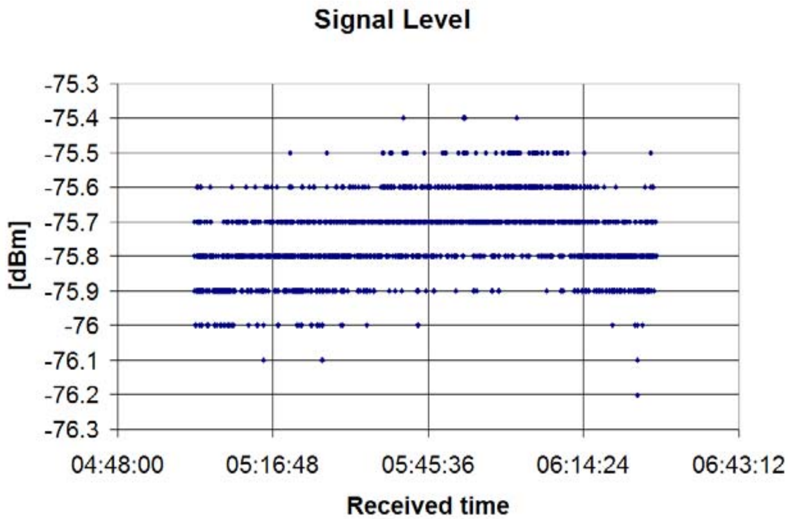

Fig. 26. Level 2 signal level (MEX-X-MRS-1-2-3-EXT2-1623-V1.0\...\DP2\M32ICL2L02_D2X_083120502_00.TAB)

4.5 Open Loop and Closed Loop data

For SCO observations the DSN provides Open Loop data and Closed Loop data. OL data is a stream of digitized voltage samples taken from the received down converted signal. A second signal is generated inside the IFMS for the down conversion. The frequency information of that signal is also stored because it is needed for the post processing of the data set.

CL data consists of a stream of the number of phase cycles counted over a defined time interval and the mean signal amplitude over the same defined time interval. There is no spectral information available. The noise associated with each value is defined by the loop bandwidth which is close to the loop filter bandwidth (the loop travel). The recorded signal frequency has also been down converted in a first stage of the CL receiver.

A: 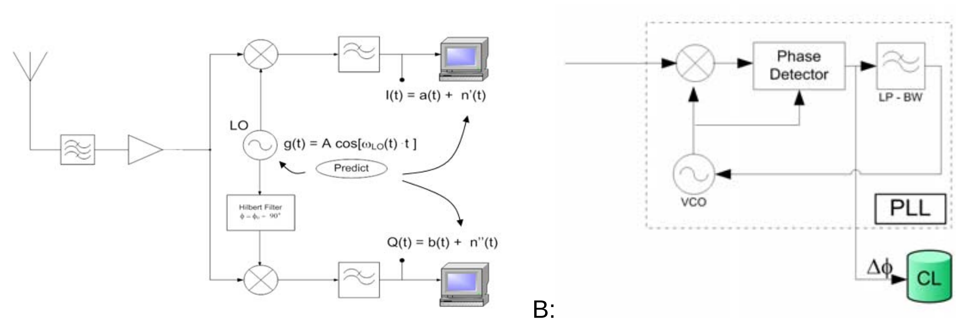 B:

Fig. 27. Schematic diagrams for OL (A) and CL (B) data recordings

The information on the two signals in both data sets allows reconstructing the real received signal with noise contributions. The OL reconstruction of the received signal is useful for extreme signal behavior that may have caused a failure in the closed loop method and therefore loss of the coherent signal at ground. In such OL data provides the possibility of reconstructing the signal and thus the TEC variation from the recorded frequency. OL data also enables analysis of scintillation and multipathing in the time and frequency range.

4.6 Brief explanation on ranging and Doppler tracking data

The two types of tracking data are briefly explained here:

- Ranging is a distance measurement based on the time difference between the time stamp of the transmitted and received code sequences (or sin wave tone frequencies) that are modulated on the carrier signal. The sequence is repeated over and over again. The code sequence length in time, multiplied by the velocity of the signal (light velocity c), gives the range for which ambiguities of the position of the S/C can be resolved. The analysis is based on the phase difference between the coherent sent and received code and independent of the coherency of the carrier signal. A good overview of the former used ESA MPTS ranging is given in RD 37 and in AD 02. An accuracy value for the IFMS ranging system is presented in RD 43 and the spacecraft transponder delay in RD 05.

- The Doppler data is based on the phase measurement of the carrier signal that is converted to a frequency value at a defined time. The transmitted frequency at time t_0 is compared with the received signal frequency at t_0 + two way light time and the difference is the measured frequency shift or “frequency shift”. This value has components that are caused by the real radial motion between transmitter and receiver, as well as by changes in the propagation medium along the ray path of the signal (RD 02).

The main difference between Doppler and range values is:

- the Doppler counts cycles of phase along the ray path versus time. The total number of cycles cannot be determined. Only the changes from a given point in time, typically the beginning of signal acquisition, can be measured.
- while range measures the group delay to an accuracy depending on the length of the sequence codes. A unique solution can be obtained for the S/C radial distance within the ambiguity associated with the highest ranging component.

4.7 Level 2 data calibration: differential Doppler

The differential Doppler data (level 2) are derived under the following approximations

- the S- and X-Band downlinks are transmitted coherently (negligible phase delays in the spacecraft transmitter and RFDU over time).
- the signals travel along the same downlink paths
- the signals are received at the same time in the ground station (path length variations vs. time in the ground station are also negligible).

The main reason for the very good quality of the differential Doppler residuals is that all oscillator variations, satellite and ground station movement related frequency shifts, and any frequency- independent delays in the path are cancelled out by calculating the difference in the change of the delay between the S- and X-Band signal. Only the plasma effect (frequency-dependent effect) is left in the residual.

It might be mentioned that in regions with a tangent point close to the Sun (inside 5 solar radii), the offset between the S- and X-Band paths can reach more than 100 km (RD 09, RD 21, RD 22). With a mean solar wind plasma velocity of 400 km/s this will cause a delay in the modulation of approx. 0.25s in regions close to the tangent point. The S-Band, which is more sensitive to the plasma and therefore refracted closer to the Sun, is modulated first by the outward moving solar wind. For the calculation of the differential Doppler this will cause a small bias in the residuals somehow proportional to the change of the plasma in this time span of 0.25s. So far it was not possible to show such an offset

4.8 Level 2 data calibration: Residual Calibrated Frequency Shifts (column 12 of the Level 2 data)

The frequency residual (residual calibrated frequency shifts) presents the difference between the real measured frequency of the received signal and the predicted received antenna frequency from a model-based calculation using the reconstructed S/C orbit [RD 02].

The calculation of the Doppler frequency shift (or the predicted received antenna frequency) is based on the reconstructed orbit file and the DE405 ephemeris.
For the calculation of the reconstructed orbit the following steps are involved in the process and taken into account (RD 32, RD 33)
:

- The reconstructed SC trajectory is the result of a calculation that searches for a trajectory giving the smallest deviation between calculated X-Band Doppler shifts based on those trajectories and the measured X-Band Doppler shifts. For MEX and VEX the trajectory fits are performed over 8 or 10 day arcs. These arcs therefore include models for the wheel-off loadings and for orbit control maneuvers.
- The calculated Doppler shifts are based on the DE405 ephemeris data for Earth, Sun and all planets
- The gravity field of the orbited planet is applied from a model with a resolution of 50X50.for the spherical harmonic expansion
- Models calculate the atmospheric drag, solar radiation pressure and thermal radiation
- Path delay corrections due to the Earth's atmosphere and ionosphere
- Relativistic effects due to massive bodies

There are no corrections done to adjust for the solar corona plasma. The orbit is thus less precise when the spacecraft are close to solar superior conjunction.
For trajectory arcs of 8 or 10 days, coronal plasma fluctuations on shorter time scales (up to days) are averaged and have a relatively small effect on the reconstructed orbit. The long-term trend of the mean plasma increase while approaching conjunction or the mean decrease while leaving conjunction, however, does produce a shift in the orbit.

The level 2 residual calibrated frequency shift as shown in Fig. 25 has an offset of 70 – 100 mHz and has a drift that is not seen in the differential Doppler data (Fig. 24). Hence, the residual calibrated frequency shifts cannot be used for the calculation of the change in TEC at this point of the analysis.

Possible further processing steps are summarized in Appendix B but the stated steps of the procedure are not tested and might give no meaningful results.

4.9 Ranging Calibration

Ranging measures the time delay (group delay) of the code between the transmit and receive times at the ground station. This includes delays due to the ground station electronic components, the spacecraft transponder and the RFDU, delays due to plasma in the path, delays due to the neutral Earth atmosphere and relativistic effects.

So far there is no calibrated ranging data on level 2 available in the archive.

The differential Ranging values must be corrected for different delays at S- and X-Band in the ground stations (for NNO see RD 44 and RD 46) and for a different S/C transponder delay (see RD 45).

4.10 Overlay of Doppler and Ranging TEC results (Calculation of TEC_0)

Example 5.3 shows the TEC values of the 2 frequency Doppler residuals calculated from the Doppler level 2 data. The 2 frequency ranging data will give a similar plot with less data points, shifted by a value TEC_0, a higher noise contribution and at different timestamps.

A possible procedure to create an overlay and to calculate TEC_0 is

- create Doppler results at the same time stamps as given in the ranging data due to an interpolation of the Doppler TEC data
- the mean value of the difference between the ranging TEC values and the interpolated Doppler TEC values gives the approximated TEC_0 value. The error on this value depends on the number of ranging points:

$$\sum_i \left(TEC_{Rang}(t_i) - TEC_{\mathrm{Dopint}}(t_i) - TEC_0 \right) \overset{!}{\cong} 0$$

$$\frac{1}{i} \sum_i \left(TEC_{Rang}(t_i) - TEC_{\mathrm{Dopint}}(t_i) \right) \cong TEC_0$$

- add the TEC_0 value to the Doppler TEC values and plot an overlay of the ranging TEC values and the Doppler TEC values. The less noisy Doppler TEC data will show up in the middle of the noisier ranging data.

4.11 List of reference documents

Lists of documents are given in the AD and RD tables. Also the processing relevant documents are part of each dataset of the PSA and can be found in the document folders.

Some general information of the Mars Express mission is also given in the 2 special ESA publications at http://sci.esa.int/ESA_SP-1240 (RD 30) and http://sci.esa.int/ESA_SP-1291 (RD 31).

4.12 Software

All level 2 data are stored as ASCII files and can be easily imported to user software programs..

The DSN level 1 data are stored in a binary format and needs special software to read and check the values of the data. A software package to translate the data is not available.

The conversion of data from level 1 to level 2 requires considerable processing. Tools for this processing step must be developed by the individual user.

5 Data processing

For further understanding of the SCO data set,,four example plots are shown here:

Example 1: SCO plane of sky plot for a whole conjunction season
Example 2: Correction for the Earth's neutral atmosphere
Example 3: Plot of the TEC variation over one tracking pass and for an entire conjunction
Example 4: Plot of the total electron density (from literature)

5.1 Example 1: Plane of sky plot

The plane of sky plot as presented here (Fig. 28) reflects the relative positions of Sun and spacecraft as viewed from Earth.

Steps used to create the plot:

- The position vectors of Earth, Sun and spacecraft are taken from the ephemeris data. The vectors are usually given in the J2000 coordinate system.
- Calculate the vectors Sun to spacecraft,, Earth to Sun, and Earth to spacecraft
- transform the vectors from J2000 to the heliocentric solar ecliptic coordinate system
- calculate the azimuth angles in the ecliptic (xy) plane for the Earth-Sun and Earth-spacecraft vectors
- calculate the elevation angles (z, above ecliptic plane) for the Earth-Sun and Earth-spacecraft vectors.
- Plot azimuth vs elevation, preferably in units of solar radii (1 degree ≈ 3.74 solar radii)

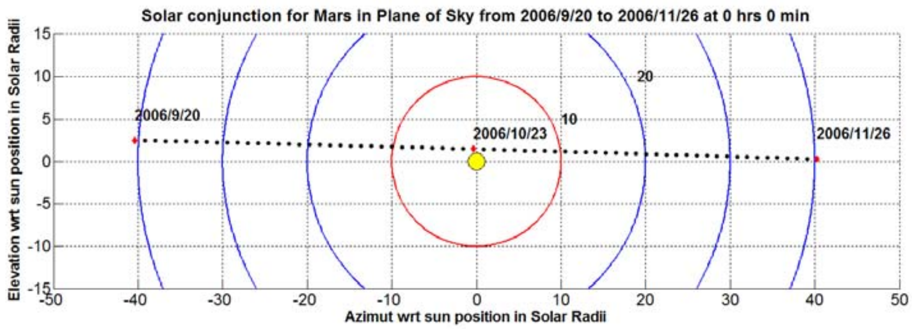

Fig. 28. Example plot for the plane of sky visualization

5.2 Example 2: Earth atmosphere correction

The Earth's atmosphere is part of the radio propagation path and the path length through the atmosphere changes over time due to the change of the antenna elevation and temperature, pressure and humidity of the air. Since the refractive index of the neutral atmosphere is not frequency dependent, a correction for the differential range or frequency is not needed. The atmospheric contribution to the delay for the one-way single-frequency (uplink or downlink) path is calculated by using standard Earth atmosphere models.
Four functions are usually created for the characterization of the neutral Earth's atmosphere:

- zenith dry model
- zenith wet model
- mapping function for the dry model
- mapping function for the wet model

Hoffman-Wellenhof describes a model (RD 35, RD 01) for the atmospheric path increase that combines the elevation angle and the vertical profile in one equation for the dry part and another equation for the wet part.
The dry part is described by

$$\Delta s_{dry}(t)=\frac{10^{-6}}{5}\frac{77.64\,\frac{p}{T}}{\sin\left(\sqrt{E^{2}+6.25}\right)}\left[40136+148.72\left(T-273.16\right)\right] \qquad (5.1)$$

And the wet part by

$$\Delta s_{wet}(t)=\frac{10^{-6}}{5}\frac{-12.96T+3.718\cdot 10^{5}}{\sin\left(\sqrt{E^{2}+2.25}\right)}\frac{e}{T^{2}}\,11000 \qquad (5.2)$$

where the elevation angle E is in deg, the temperature T in kelvin, the pressure p in mbar, and the water vapour partial pressure e in hpascal.

The relation between the relative humidity h [%], as given in the meteo files, and the water vapour partial pressure *e* is

$$e = 6.108 \cdot 10^{-2} \cdot h \cdot e^{\frac{17.393(T-273.15)}{T-33.95}} \tag{5.3}$$

The total time delay for the up and downlink is then

$$\tau_{Tropsphere} = \frac{1}{c}\left[\left(\Delta s_{dry} + \Delta s_{wet}\right)_{uplink} + \left(\Delta s_{dry} + \Delta s_{wet}\right)_{downlink}\right] \tag{5.4}$$

A plot of the frequency shift and the path delay change is shown in Fig. 29.

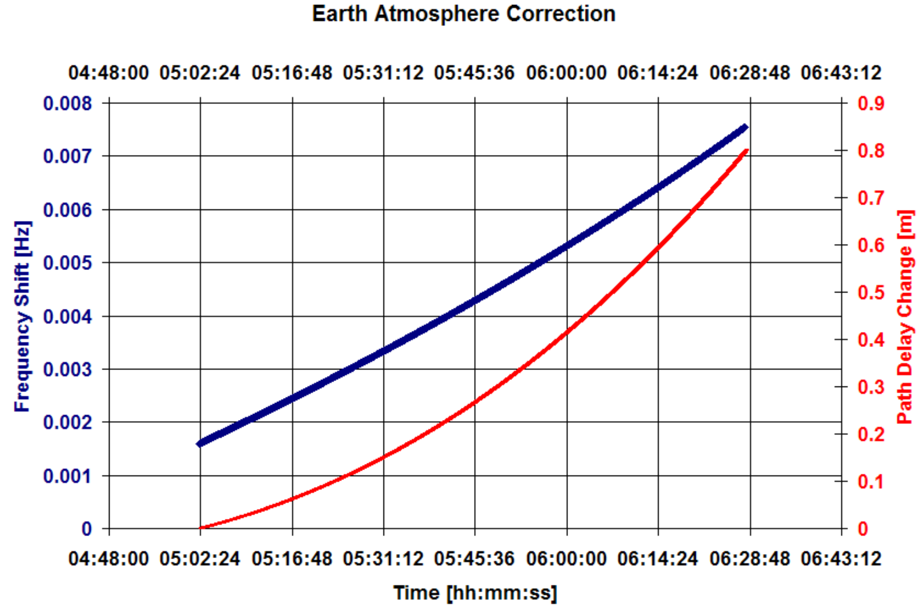

Fig. 29. Level 2 earth atmosphere correction for the frequency residuals. The blue values represent the frequency shift and the red values the path delay change for this 1.5h. (MEX-X-MRS-1-2-3-EXT2-1623-V1.0\...\DP2\M32ICL2L02_D2X_083120502_00.TAB)

5.3 Example 3: TEC plot

The Total Electron Content given by equation (3.16) using the differential Doppler level 2 data is shown in Fig. 30 for the MEX tracking pass on DOY 312 2008. There is no differential ranging data set available that could have been used to calculate TEC_0.

$$\boxed{TEC = \left[\frac{40.31}{c}\, f_S \left(\frac{1}{f_S^2} - \frac{1}{f_X^2}\right)\right]^{-1} \int_{t_0}^{t} \Delta f_{Plasma}\, dt + TEC_0}$$

The solar-induced variations of the TEC are well above the noise level and therefore a useful product for further analysis.

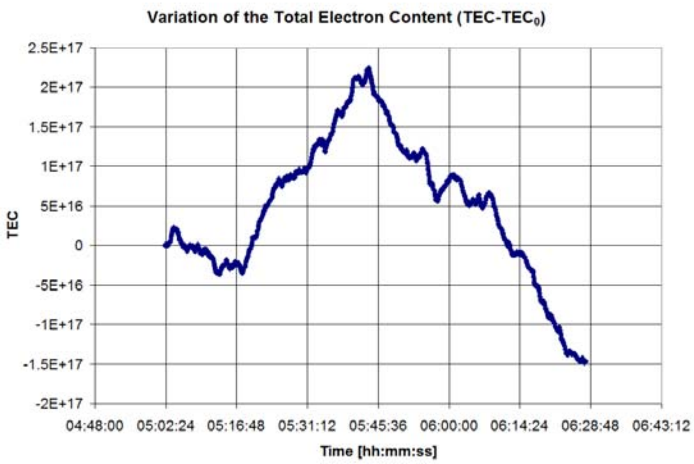

Fig. 30. Variation of the TEC vs. time. The integrated differential Doppler shows the variation of the total amount of electrons in the path. The absolute value of the column density can only be calculated with differential ranging values. (MEX-X-MRS-1-2-3-EXT2-1623-V1.0\...\DP2\M32ICL2L02_D2X_083120502_00.TAB)

The differential ranging values during a whole conjunction period with will show how the TEC is changing with respect to the distance of the ray path proximate point to the Sun. Fig. 31 shows the results of the dual-frequency ranging measurements recorded during the Ulysses 1991 conjunction. A mean value of the TEC is computed for each tracking pass and the data are fit separately to equation (3.21) for both egress and ingress phases.

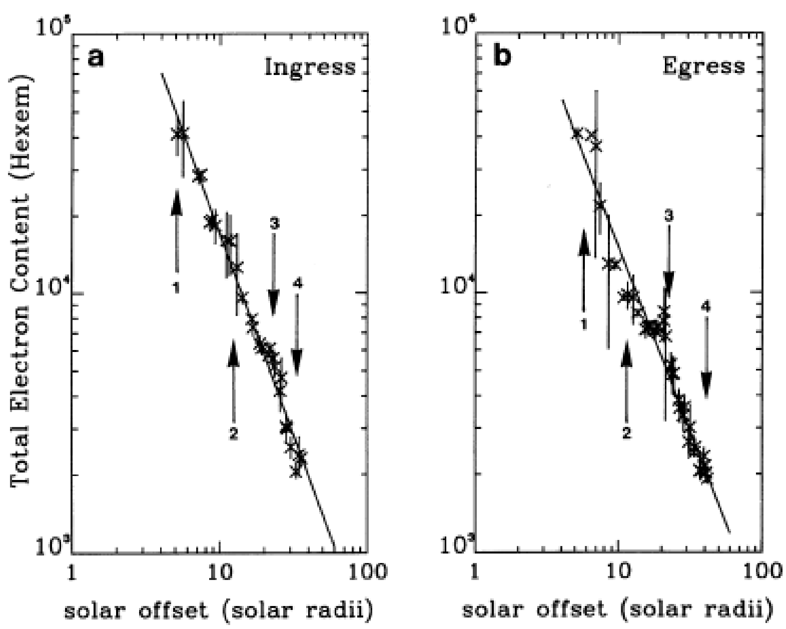

Fig. 31. TEC as function of the ray path proximate point distance to the Sun (RD 15).

5.4 Example 4: Coronal electron density plot

The total number of electrons as available in the level 2 differential ranging data is also needed to calculate the approx. electron density of the tangent point and therefore the density change with respect to the distance to the sun. It is possible to do this via a regression fit method used on the total electron content as explained in 5.3 or the Abel inversion can be used on the integral in equation (3.2).

$$\Delta s_{Plasma} = \frac{40.3}{f^2} \int_0^s N_e \, ds$$

Both methods are based on a spherical electron density distribution. Fig. 32 shows some results of conjunctions done on various missions. More details regarding the image are given in RD 36.

The Abel inversion is discussed in detail in literature while used for example in the field of tomography and atmosphere sounding. It is not described here.

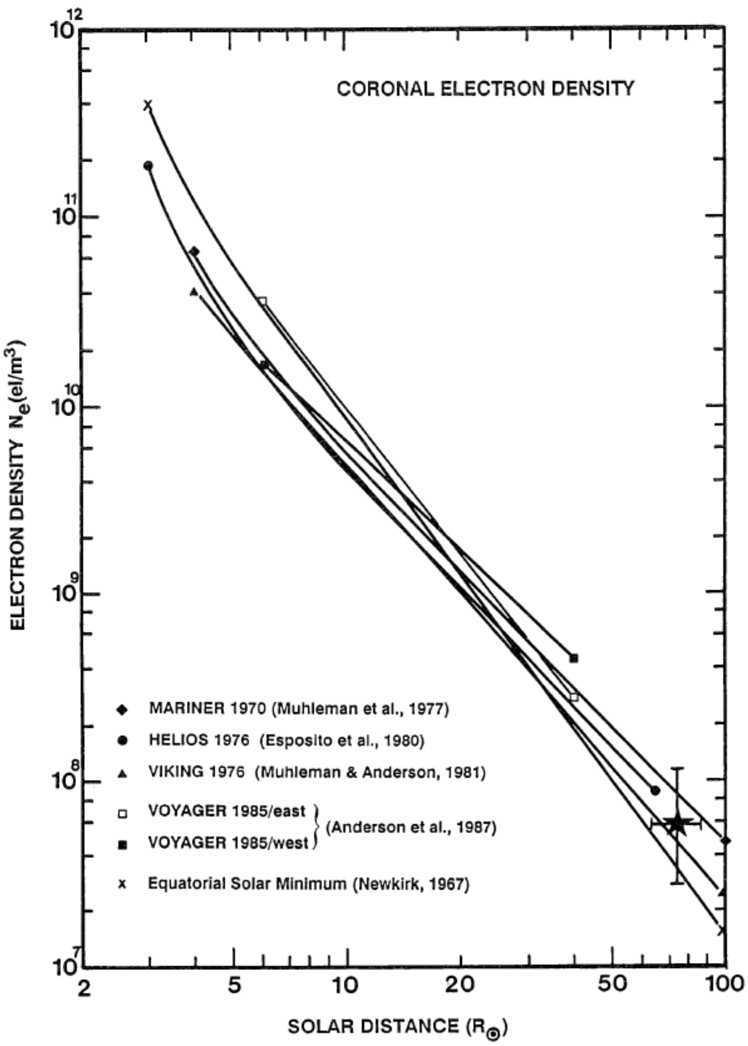

Fig. 32. An example for the electron density as a function of solar distance in sun radii (RD 36).

Acknoledgement:

It is a pleasure to thank the MEX project scientist Olivier Witasse, who initiated this work, and the mission manager Fred Jansen, for their support. Special thanks go to the radio science teams, led by Martin Pätzold on MEX and Rosetta, and Bernd Häusler on VEX. I have also received support from Michael Bird and have had many interesting discussions with Matthias Hahn, both members of the radio science team working on various topics with the SCO data.

Appendices

A. List of available Solar Corona Experiment data in the PSA

The list below is extracted from the aareadme.txt file of the Mars Express folder ftp://psa.esac.esa.int/pub/mirror/MARS-EXPRESS/MRS/MEX-M-MRS-1-2-3-EXT2-2950-V1.0 and reflects the archived data until:

PUBLICATION_DATE = 2012-03-02

- **MEX SCO 2004**

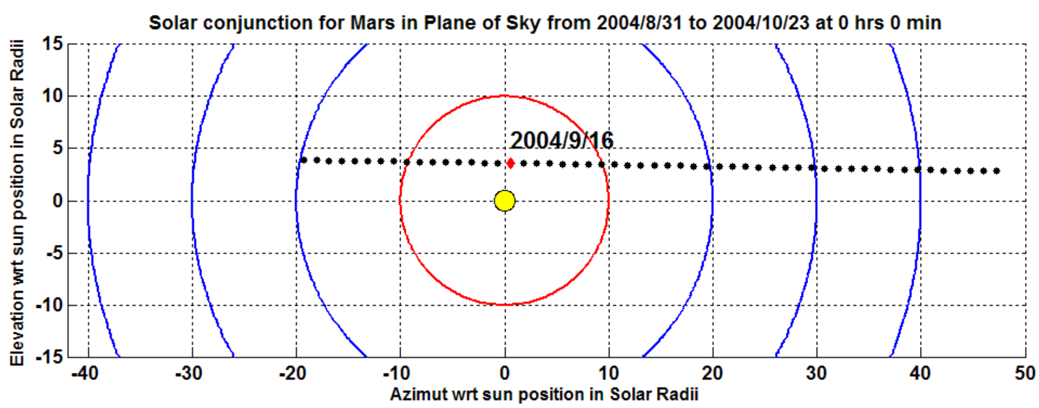

Fig. 33. MEX SCO 2004 plane of sky plot. The position of MEX is shown for each day from the first day of data to the last day. The red dot marks the date of solar conjunction.

PSA Dataset Name	RSI Volume ID	Start Date	End Date	Notes
MEX-X-MRS-1/2/3-PRM-0147-V1.0	MEXMRS_0124	31.08.2004	31.08.2004	Solar Conjunction
MEX-X-MRS-1/2/3-PRM-0148-V1.0	MEXMRS_0128	25.08.2004	25.08.2004	Solar Conjunction

MEX-X-MRS-1/2/3-PRM-0128-V1.0	MEXMRS_0147	18.08.2004	18.08.2004	Solar Conjunction
MEX-X-MRS-1/2/3-PRM-0149-V1.0	MEXMRS_0148	21.08.2004	21.08.2004	Solar Conjunction
MEX-X-MRS-1/2/3-PRM-0150-V1.0	MEXMRS_0149	28.08.2004	28.08.2004	Solar Conjunction
MEX-X-MRS-1/2/3-PRM-0151-V1.0	MEXMRS_0150	29.08.2004	29.08.2004	Solar Conjunction
MEX-X-MRS-1/2/3-PRM-0124-V1.0	MEXMRS_0151	30.08.2004	30.08.2004	Solar Conjunction
MEX-X-MRS-1/2/3-PRM-0152-V1.0	MEXMRS_0152	01.09.2004	01.09.2004	Solar Conjunction
MEX-X-MRS-1/2/3-PRM-0153-V1.0	MEXMRS_0153	03.09.2004	03.09.2004	Solar Conjunction
MEX-X-MRS-1/2/3-PRM-0154-V1.0	MEXMRS_0154	04.09.2004	04.09.2004	Solar Conjunction
MEX-X-MRS-1/2/3-PRM-0155-V1.0	MEXMRS_0155	05.09.2004	05.09.2004	Solar Conjunction
MEX-X-MRS-1/2/3-PRM-0156-V1.0	MEXMRS_0156	06.09.2004	06.09.2004	Solar Conjunction
MEX-X-MRS-1/2/3-PRM-0157-V1.0	MEXMRS_0157	06.09.2004	06.09.2004	Solar Conjunction
MEX-X-MRS-1/2/3-PRM-0159-V1.0	MEXMRS_0159	08.09.2004	08.09.2004	Solar Conjunction
MEX-X-MRS-1/2/3-PRM-0160-V1.0	MEXMRS_0160	10.09.2004	10.09.2004	Solar Conjunction
MEX-X-MRS-1/2/3-PRM-0161-V1.0	MEXMRS_0161	11.09.2004	11.09.2004	Solar Conjunction
MEX-X-MRS-1/2/3-PRM-0162-V1.0	MEXMRS_0162	12.09.2004	12.09.2004	Solar Conjunction
MEX-X-MRS-1/2/3-PRM-0163-V1.0	MEXMRS_0163	13.09.2004	13.09.2004	Solar Conjunction
MEX-X-MRS-1/2/3-PRM-0166-V1.0	MEXMRS_0166	17.09.2004	17.09.2004	Solar Conjunction
MEX-X-MRS-1/2/3-PRM-0167-V1.0	MEXMRS_0167	18.09.2004	18.09.2004	Solar Conjunction
MEX-X-MRS-1/2/3-PRM-0168-V1.0	MEXMRS_0168	18.09.2004	18.09.2004	Solar Conjunction
MEX-X-MRS-1/2/3-PRM-0169-V1.0	MEXMRS_0169	19.09.2004	19.09.2004	Solar Conjunction
MEX-X-MRS-1/2/3-PRM-0170-V1.0	MEXMRS_0170	20.09.2004	20.09.2004	Solar Conjunction

MEX-X-MRS-1/2/3-PRM-0171-V1.0	MEXMRS_0171	21.09.2004	21.09.2004	Solar Conjunction
MEX-X-MRS-1/2/3-PRM-0173-V1.0	MEXMRS_0173	23.09.2004	23.09.2004	Solar Conjunction
MEX-X-MRS-1/2/3-PRM-0174-V1.0	MEXMRS_0174	24.09.2004	24.09.2004	Solar Conjunction
MEX-X-MRS-1/2/3-PRM-0175-V1.0	MEXMRS_0175	25.09.2004	25.09.2004	Solar Conjunction
MEX-X-MRS-1/2/3-PRM-0177-V1.0	MEXMRS_0177	28.09.2004	28.09.2004	Solar Conjunction
MEX-X-MRS-1/2/3-PRM-0178-V1.0	MEXMRS_0178	01.10.2004	01.10.2004	Solar Conjunction
MEX-X-MRS-1/2/3-PRM-0180-V1.0	MEXMRS_0180	05.10.2004	05.10.2004	Solar Conjunction
MEX-X-MRS-1/2/3-PRM-0181-V1.0	MEXMRS_0181	10.10.2004	10.10.2004	Solar Conjunction
MEX-X-MRS-1/2/3-PRM-0182-V1.0	MEXMRS_0182	12.10.2004	12.10.2004	Solar Conjunction
MEX-X-MRS-1/2/3-PRM-0183-V1.0	MEXMRS_0183	13.10.2004	13.10.2004	Solar Conjunction
MEX-X-MRS-1/2/3-PRM-0184-V1.0	MEXMRS_0184	15.10.2004	15.10.2004	Solar Conjunction
MEX-X-MRS-1/2/3-PRM-0189-V1.0	MEXMRS_0189	22.10.2004	22.10.2004	Solar Conjunction

- **MEX SCO 2006**

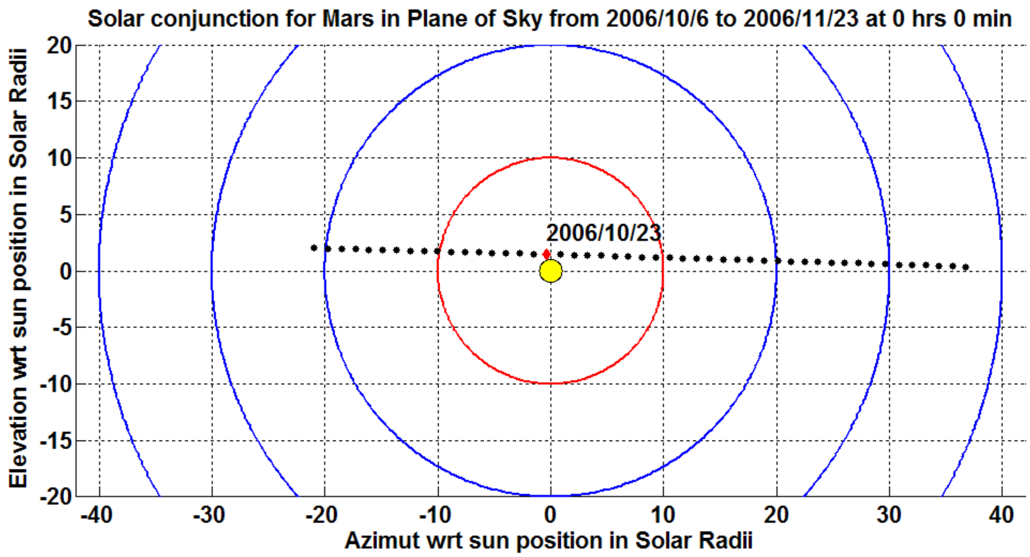

Fig. 34. MEX SCO 2006 plane of sky plot (similar to Fig. 33).

PSA Dataset Name	RSI Volume ID	Volume ID	Start Date	Notes
MEX-X-MRS-1/2/3-EXT1-1048-V1.0	MEXMRS_1048	MEXMRS_2185	06.10.2006	Solar Conjunction
MEX-X-MRS-1/2/3-EXT1-1049-V1.0	MEXMRS_1049	MEXMRS_3030	07.10.2006	Solar Conjunction
MEX-X-MRS-1/2/3-EXT1-1050-V1.0	MEXMRS_1050	MEXMRS_3002	07.10.2006	Solar Conjunction
MEX-X-MRS-1/2/3-EXT1-1051-V1.0	MEXMRS_1051	MEXMRS_3001	08.10.2006	Solar Conjunction
MEX-X-MRS-1/2/3-EXT1-1052-V1.0	MEXMRS_1052	MEXMRS_3000	09.10.2006	Solar Conjunction
MEX-X-MRS-1/2/3-EXT1-1053-V1.0	MEXMRS_1053	MEXMRS_3003	10.10.2006	Solar Conjunction
MEX-X-MRS-1/2/3-EXT1-1054-V1.0	MEXMRS_1054	MEXMRS_3004	11.10.2006	Solar Conjunction
MEX-X-MRS-1/2/3-EXT1-1056-V1.0	MEXMRS_1056	MEXMRS_3005	13.10.2006	Solar Conjunction
MEX-X-MRS-1/2/3-EXT1-1057-V1.0	MEXMRS_1057	MEXMRS_3006	14.10.2006	Solar Conjunction
MEX-X-MRS-1/2/3-EXT1-1058-V1.0	MEXMRS_1058	MEXMRS_3007	14.10.2006	Solar Conjunction
MEX-X-MRS-1/2/3-EXT1-1059-V1.0	MEXMRS_1059	MEXMRS_3015	15.10.2006	Solar Conjunction

MEX-X-MRS-1/2/3-EXT1-1061-V1.0	MEXMRS_1061	MEXMRS_3008	17.10.2006	Solar Conjunction
MEX-X-MRS-1/2/3-EXT1-1063-V1.0	MEXMRS_1063	MEXMRS_3009	18.10.2006	Solar Conjunction
MEX-X-MRS-1/2/3-EXT1-1072-V1.0	MEXMRS_1072	MEXMRS_3010	31.10.2006	Solar Conjunction
MEX-X-MRS-1/2/3-EXT1-1073-V1.0	MEXMRS_1073	MEXMRS_3011	06.11.2006	Solar Conjunction
MEX-X-MRS-1/2/3-EXT1-1074-V1.0	MEXMRS_1074	MEXMRS_3012	07.11.2006	Solar Conjunction
MEX-X-MRS-1/2/3-EXT1-1075-V1.0	MEXMRS_1075	MEXMRS_3013	08.11.2006	Solar Conjunction
MEX-X-MRS-1/2/3-EXT1-1076-V1.0	MEXMRS_1076	MEXMRS_3014	11.11.2006	Solar Conjunction
MEX-X-MRS-1/2/3-EXT1-1077-V1.0	MEXMRS_1077	MEXMRS_3016	12.11.2006	Solar Conjunction
MEX-X-MRS-1/2/3-EXT1-1078-V1.0	MEXMRS_1078	MEXMRS_3022	13.11.2006	Solar Conjunction
MEX-X-MRS-1/2/3-EXT1-1079-V1.0	MEXMRS_1079	MEXMRS_3021	14.11.2006	Solar Conjunction
MEX-X-MRS-1/2/3-EXT1-1080-V1.0	MEXMRS_1080	MEXMRS_3023	15.11.2006	Solar Conjunction
MEX-X-MRS-1/2/3-EXT1-1081-V1.0	MEXMRS_1081	MEXMRS_3024	17.11.2006	Solar Conjunction
MEX-X-MRS-1/2/3-EXT1-1082-V1.0	MEXMRS_1082	MEXMRS_3026	18.11.2006	Solar Conjunction
MEX-X-MRS-1/2/3-EXT1-1083-V1.0	MEXMRS_1083	MEXMRS_3025	19.11.2006	Solar Conjunction
MEX-X-MRS-1/2/3-EXT1-1085-V1.0	MEXMRS_1085	MEXMRS_3028	21.11.2006	Solar Conjunction
MEX-X-MRS-1/2/3-EXT1-1086-V1.0	MEXMRS_1086	MEXMRS_3029	22.11.2006	Solar Conjunction

- **MEX SCO 2008**

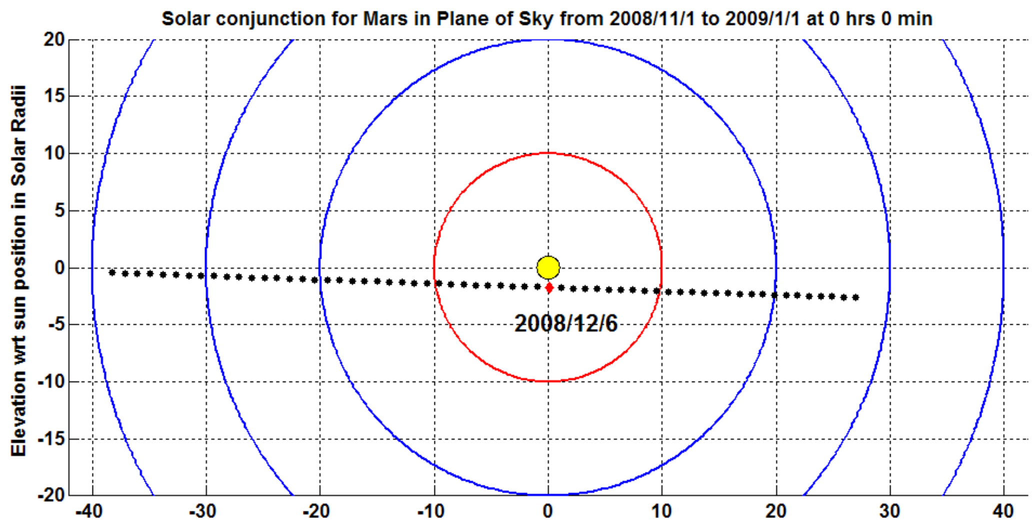

Fig. 35. MEX SCO 2008 plane of sky plot (similar to Fig. 33).

PSA Dataset Name	RSI Volume ID	Volume ID	Start Date	Notes
MEX-X-MRS-1/2/3-EXT2-1613-V1.0	MEXMRS_1613	MEXMRS_3035	01.11.2008	Solar Conjunction
MEX-X-MRS-1/2/3-EXT2-1614-V1.0	MEXMRS_1614	MEXMRS_3117	01.11.2008	Solar Conjunction
MEX-X-MRS-1/2/3-EXT2-1616-V1.0	MEXMRS_1616	MEXMRS_3036	02.11.2008	Solar Conjunction
MEX-X-MRS-1/2/3-EXT2-1618-V1.0	MEXMRS_1618	MEXMRS_3037	03.11.2008	Solar Conjunction
MEX-X-MRS-1/2/3-EXT2-1622-V1.0	MEXMRS_1622	MEXMRS_3038	06.11.2008	Solar Conjunction
MEX-X-MRS-1/2/3-EXT2-1623-V1.0	MEXMRS_1623	MEXMRS_3039	07.11.2008	Solar Conjunction
MEX-X-MRS-1/2/3-EXT2-1624-V1.0	MEXMRS_1624	MEXMRS_3040	08.11.2008	Solar Conjunction
MEX-X-MRS-1/2/3-EXT2-1625-V1.0	MEXMRS_1625	MEXMRS_3045	08.11.2008	Solar Conjunction
MEX-X-MRS-1/2/3-EXT2-1626-V1.0	MEXMRS_1626	MEXMRS_3068	09.11.2008	Solar Conjunction
MEX-X-MRS-1/2/3-EXT2-1631-V1.0	MEXMRS_1631	MEXMRS_3069	14.11.2008	Solar Conjunction
MEX-X-MRS-1/2/3-EXT2-1632-V1.0	MEXMRS_1632	MEXMRS_3067	15.11.2008	Solar Conjunction
MEX-X-MRS-1/2/3-EXT2-1633-V1.0	MEXMRS_1633	MEXMRS_3041	15.11.2008	Solar Conjunction
MEX-X-MRS-1/2/3-EXT2-1635-V1.0	MEXMRS_1635	MEXMRS_3042	16.11.2008	Solar Conjunction
MEX-X-MRS-1/2/3-EXT2-1636-V1.0	MEXMRS_1636	MEXMRS_3043	16.11.2008	Solar Conjunction
MEX-X-MRS-1/2/3-EXT2-1638-V1.0	MEXMRS_1638	MEXMRS_3046	17.11.2008	Solar Conjunction
MEX-X-MRS-1/2/3-EXT2-1639-V1.0	MEXMRS_1639	MEXMRS_3245	19.11.2008	Solar Conjunction
MEX-X-MRS-1/2/3-EXT2-1640-V1.0	MEXMRS_1640	MEXMRS_3081	20.11.2008	Solar Conjunction
MEX-X-MRS-1/2/3-EXT2-1641-V1.0	MEXMRS_1641	MEXMRS_3118	15.11.2008	Solar Conjunction
MEX-X-MRS-1/2/3-EXT2-1642-V1.0	MEXMRS_1642	MEXMRS_3082	21.11.2008	Solar Conjunction
MEX-X-MRS-1/2/3-EXT2-1643-V1.0	MEXMRS_1643	MEXMRS_3044	21.11.2008	Solar Conjunction
MEX-X-MRS-1/2/3-EXT2-1644-V1.0	MEXMRS_1644	MEXMRS_3083	22.11.2008	Solar Conjunction

MEX-X-MRS-1/2/3-EXT2-1645-V1.0	MEXMRS_1645	MEXMRS_3246	22.11.2008	Solar Conjunction
MEX-X-MRS-1/2/3-EXT2-1646-V1.0	MEXMRS_1646	MEXMRS_3084	23.11.2008	Solar Conjunction
MEX-X-MRS-1/2/3-EXT2-1647-V1.0	MEXMRS_1647	MEXMRS_3247	23.11.2008	Solar Conjunction
MEX-X-MRS-1/2/3-EXT2-1648-V1.0	MEXMRS_1648	MEXMRS_3085	24.11.2008	Solar Conjunction
MEX-X-MRS-1/2/3-EXT2-1649-V1.0	MEXMRS_1649	MEXMRS_3248	25.11.2008	Solar Conjunction
MEX-X-MRS-1/2/3-EXT2-1650-V1.0	MEXMRS_1650	MEXMRS_3086	25.11.2008	Solar Conjunction
MEX-X-MRS-1/2/3-EXT2-1651-V1.0	MEXMRS_1651	MEXMRS_3249	25.11.2008	Solar Conjunction
MEX-X-MRS-1/2/3-EXT2-1652-V1.0	MEXMRS_1652	MEXMRS_3087	26.11.2008	Solar Conjunction
MEX-X-MRS-1/2/3-EXT2-1653-V1.0	MEXMRS_1653	MEXMRS_3088	26.11.2008	Solar Conjunction
MEX-X-MRS-1/2/3-EXT2-1654-V1.0	MEXMRS_1654	MEXMRS_3250	26.11.2008	Solar Conjunction
MEX-X-MRS-1/2/3-EXT2-1656-V1.0	MEXMRS_1656	MEXMRS_3251	27.11.2008	Solar Conjunction
MEX-X-MRS-1/2/3-EXT2-1658-V1.0	MEXMRS_1658	MEXMRS_3090	28.11.2008	Solar Conjunction
MEX-X-MRS-1/2/3-EXT2-1659-V1.0	MEXMRS_1659	MEXMRS_3252	29.11.2008	Solar Conjunction
MEX-X-MRS-1/2/3-EXT2-1660-V1.0	MEXMRS_1660	MEXMRS_3091	29.11.2008	Solar Conjunction
MEX-X-MRS-1/2/3-EXT2-1661-V1.0	MEXMRS_1661	MEXMRS_3092	29.11.2008	Solar Conjunction
MEX-X-MRS-1/2/3-EXT2-1662-V1.0	MEXMRS_1662	MEXMRS_3070	30.11.2008	Solar Conjunction
MEX-X-MRS-1/2/3-EXT2-1663-V1.0	MEXMRS_1663	MEXMRS_3093	30.11.2008	Solar Conjunction
MEX-X-MRS-1/2/3-EXT2-1664-V1.0	MEXMRS_1664	MEXMRS_3253	30.11.2008	Solar Conjunction
MEX-X-MRS-1/2/3-EXT2-1665-V1.0	MEXMRS_1665	MEXMRS_3094	01.12.2008	Solar Conjunction
MEX-X-MRS-1/2/3-EXT2-1677-V1.0	MEXMRS_1677	MEXMRS_3061	07.12.2008	Solar Conjunction
MEX-X-MRS-1/2/3-EXT2-1678-V1.0	MEXMRS_1678	MEXMRS_3100	08.12.2008	Solar Conjunction
MEX-X-MRS-1/2/3-EXT2-1680-V1.0	MEXMRS_1680	MEXMRS_3062	09.12.2008	Solar Conjunction
MEX-X-MRS-1/2/3-EXT2-1681-V1.0	MEXMRS_1681	MEXMRS_3101	10.12.2008	Solar Conjunction
MEX-X-MRS-1/2/3-EXT2-1682-V1.0	MEXMRS_1682	MEXMRS_3063	10.12.2008	Solar Conjunction
MEX-X-MRS-1/2/3-EXT2-1683-V1.0	MEXMRS_1683	MEXMRS_3102	11.12.2008	Solar Conjunction
MEX-X-MRS-1/2/3-EXT2-1684-V1.0	MEXMRS_1684	MEXMRS_3064	11.12.2008	Solar Conjunction
MEX-X-MRS-1/2/3-EXT2-1686-V1.0	MEXMRS_1686	MEXMRS_3255	12.12.2008	Solar Conjunction
MEX-X-MRS-1/2/3-EXT2-1687-V1.0	MEXMRS_1687	MEXMRS_3103	13.12.2008	Solar Conjunction
MEX-X-MRS-1/2/3-EXT2-1688-V1.0	MEXMRS_1688	MEXMRS_3073	14.12.2008	Solar Conjunction
MEX-X-MRS-1/2/3-EXT2-1689-V1.0	MEXMRS_1689	MEXMRS_3104	14.12.2008	Solar Conjunction
MEX-X-MRS-1/2/3-EXT2-1690-V1.0	MEXMRS_1690	MEXMRS_3074	14.12.2008	Solar Conjunction
MEX-X-MRS-1/2/3-EXT2-1691-V1.0	MEXMRS_1691	MEXMRS_3105	15.12.2008	Solar Conjunction
MEX-X-MRS-1/2/3-EXT2-1694-V1.0	MEXMRS_1694	MEXMRS_3254	17.12.2008	Solar Conjunction
MEX-X-MRS-1/2/3-EXT2-1696-V1.0	MEXMRS_1696	MEXMRS_3106	17.12.2008	Solar Conjunction
MEX-X-MRS-1/2/3-EXT2-1697-V1.0	MEXMRS_1697	MEXMRS_3066	17.12.2008	Solar Conjunction

MEX-X-MRS-1/2/3-EXT2-1698-V1.0	MEXMRS_1698	MEXMRS_3107	18.12.2008	Solar Conjunction
MEX-X-MRS-1/2/3-EXT2-1699-V1.0	MEXMRS_1699	MEXMRS_3075	18.12.2008	Solar Conjunction
MEX-X-MRS-1/2/3-EXT2-1700-V1.0	MEXMRS_1700	MEXMRS_3108	19.12.2008	Solar Conjunction
MEX-X-MRS-1/2/3-EXT2-1701-V1.0	MEXMRS_1701	MEXMRS_3076	19.12.2008	Solar Conjunction
MEX-X-MRS-1/2/3-EXT2-1702-V1.0	MEXMRS_1702	MEXMRS_3052	21.12.2008	Solar Conjunction
MEX-X-MRS-1/2/3-EXT2-1703-V1.0	MEXMRS_1703	MEXMRS_3109	21.12.2008	Solar Conjunction
MEX-X-MRS-1/2/3-EXT2-1705-V1.0	MEXMRS_1705	MEXMRS_3053	22.12.2008	Solar Conjunction
MEX-X-MRS-1/2/3-EXT2-1707-V1.0	MEXMRS_1707	MEXMRS_3077	23.12.2008	Solar Conjunction
MEX-X-MRS-1/2/3-EXT2-1709-V1.0	MEXMRS_1709	MEXMRS_3054	24.12.2008	Solar Conjunction
MEX-X-MRS-1/2/3-EXT2-1710-V1.0	MEXMRS_1710	MEXMRS_3078	25.12.2008	Solar Conjunction
MEX-X-MRS-1/2/3-EXT2-1712-V1.0	MEXMRS_1712	MEXMRS_3055	25.12.2008	Solar Conjunction
MEX-X-MRS-1/2/3-EXT2-1713-V1.0	MEXMRS_1713	MEXMRS_3056	26.12.2008	Solar Conjunction
MEX-X-MRS-1/2/3-EXT2-1714-V1.0	MEXMRS_1714	MEXMRS_3065	26.12.2008	Solar Conjunction
MEX-X-MRS-1/2/3-EXT2-1715-V1.0	MEXMRS_1715	MEXMRS_3057	27.12.2008	Solar Conjunction
MEX-X-MRS-1/2/3-EXT2-1716-V1.0	MEXMRS_1716	MEXMRS_3111	27.12.2008	Solar Conjunction
MEX-X-MRS-1/2/3-EXT2-1717-V1.0	MEXMRS_1717	MEXMRS_3058	28.12.2008	Solar Conjunction
MEX-X-MRS-1/2/3-EXT2-1718-V1.0	MEXMRS_1718	MEXMRS_3079	28.12.2008	Solar Conjunction
MEX-X-MRS-1/2/3-EXT2-1719-V1.0	MEXMRS_1719	MEXMRS_3112	28.12.2008	Solar Conjunction
MEX-X-MRS-1/2/3-EXT2-1720-V1.0	MEXMRS_1720	MEXMRS_3059	28.12.2008	Solar Conjunction
MEX-X-MRS-1/2/3-EXT2-1722-V1.0	MEXMRS_1722	MEXMRS_3113	29.12.2008	Solar Conjunction
MEX-X-MRS-1/2/3-EXT2-1723-V1.0	MEXMRS_1723	MEXMRS_3060	29.12.2008	Solar Conjunction
MEX-X-MRS-1/2/3-EXT2-1725-V1.0	MEXMRS_1725	MEXMRS_3114	31.12.2008	Solar Conjunction
MEX-X-MRS-1/2/3-EXT2-1727-V1.0	MEXMRS_1727	MEXMRS_3119	01.01.2009	Solar Conjunction
MEX-X-MRS-1/2/3-EXT2-1729-V1.0	MEXMRS_1729	MEXMRS_3120	02.01.2009	Solar Conjunction
MEX-X-MRS-1/2/3-EXT2-1730-V1.0	MEXMRS_1730	MEXMRS_3121	02.01.2009	Solar Conjunction
MEX-X-MRS-1/2/3-EXT2-1732-V1.0	MEXMRS_1732	MEXMRS_3122	02.01.2009	Solar Conjunction
MEX-X-MRS-1/2/3-EXT2-1733-V1.0	MEXMRS_1733	MEXMRS_3123	03.01.2009	Solar Conjunction
MEX-X-MRS-1/2/3-EXT2-1734-V1.0	MEXMRS_1734	MEXMRS_3124	03.01.2009	Solar Conjunction
MEX-X-MRS-1/2/3-EXT2-1735-V1.0	MEXMRS_1735	MEXMRS_3125	04.01.2009	Solar Conjunction
MEX-X-MRS-1/2/3-EXT2-1738-V1.0	MEXMRS_1738	MEXMRS_3126	05.01.2009	Solar Conjunction
MEX-X-MRS-1/2/3-EXT2-1739-V1.0	MEXMRS_1739	MEXMRS_3127	05.01.2009	Solar Conjunction
MEX-X-MRS-1/2/3-EXT2-1742-V1.0	MEXMRS_1742	MEXMRS_3128	07.01.2009	Solar Conjunction
MEX-X-MRS-1/2/3-EXT2-1743-V1.0	MEXMRS_1743	MEXMRS_3129	08.01.2009	Solar Conjunction
MEX-X-MRS-1/2/3-EXT2-1744-V1.0	MEXMRS_1744	MEXMRS_3130	08.01.2009	Solar Conjunction
MEX-X-MRS-1/2/3-EXT2-1746-V1.0	MEXMRS_1746	MEXMRS_3131	09.01.2009	Solar Conjunction

MEX-X-MRS-1/2/3-EXT2-1747-V1.0	MEXMRS_1747	MEXMRS_3132	10.01.2009	Solar Conjunction
MEX-X-MRS-1/2/3-EXT2-1748-V1.0	MEXMRS_1748	MEXMRS_3133	10.01.2009	Solar Conjunction
MEX-X-MRS-1/2/3-EXT2-1749-V1.0	MEXMRS_1749	MEXMRS_3134	10.01.2009	Solar Conjunction
MEX-X-MRS-1/2/3-EXT2-1751-V1.0	MEXMRS_1751	MEXMRS_3135	12.01.2009	Solar Conjunction
MEX-X-MRS-1/2/3-EXT2-1752-V1.0	MEXMRS_1752	MEXMRS_3136	13.01.2009	Solar Conjunction
MEX-X-MRS-1/2/3-EXT2-1753-V1.0	MEXMRS_1753	MEXMRS_3137	14.01.2009	Solar Conjunction
MEX-X-MRS-1/2/3-EXT2-1756-V1.0	MEXMRS_1756	MEXMRS_3138	15.01.2009	Solar Conjunction

- **MEX SCO 2010 - 2011**

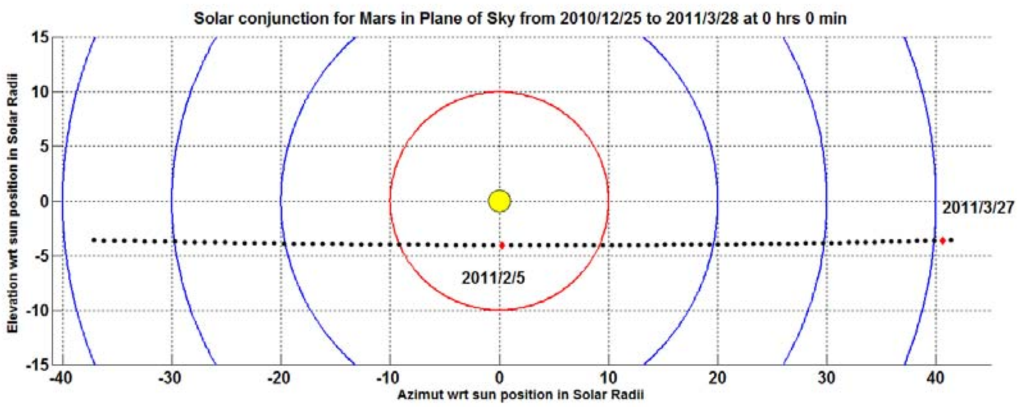

Fig. 36. MEX SCO 2010 - 2011 plane of sky plot. The position of MEX is shown for each day in the solar offset range between +/- 40 solar radii. The central red dot marks the date of solar conjunction.

PSA Dataset Name	RSI Volume ID	Volume ID	Start Date	Notes
MEX-X-MRS-1/2/3-EXT2-2696-V1.0	MEXMRS_2696	MEXMRS_3139	25.12.2010	Solar Conjunction
MEX-X-MRS-1/2/3-EXT2-2697-V1.0	MEXMRS_2697	MEXMRS_3140	26.12.2010	Solar Conjunction
MEX-X-MRS-1/2/3-EXT2-2698-V1.0	MEXMRS_2698	MEXMRS_3141	26.12.2010	Solar Conjunction
MEX-X-MRS-1/2/3-EXT2-2699-V1.0	MEXMRS_2699	MEXMRS_3142	26.12.2010	Solar Conjunction
MEX-X-MRS-1/2/3-EXT2-2700-V1.0	MEXMRS_2700	MEXMRS_3143	27.12.2010	Solar Conjunction
MEX-X-MRS-1/2/3-EXT2-2701-V1.0	MEXMRS_2701	MEXMRS_3144	28.12.2010	Solar Conjunction
MEX-X-MRS-1/2/3-EXT2-2702-V1.0	MEXMRS_2702	MEXMRS_3145	28.12.2010	Solar Conjunction
MEX-X-MRS-1/2/3-EXT2-2703-V1.0	MEXMRS_2703	MEXMRS_3146	29.12.2010	Solar Conjunction
MEX-X-MRS-1/2/3-EXT2-2704-V1.0	MEXMRS_2704	MEXMRS_3147	30.12.2010	Solar Conjunction
MEX-X-MRS-1/2/3-EXT2-2705-V1.0	MEXMRS_2705	MEXMRS_3148	31.12.2010	Solar Conjunction

MEX-X-MRS-1/2/3-EXT2-2706-V1.0	MEXMRS_2706	MEXMRS_3149	01.01.2011	Solar Conjunction
MEX-X-MRS-1/2/3-EXT2-2707-V1.0	MEXMRS_2707	MEXMRS_3150	01.01.2011	Solar Conjunction
MEX-X-MRS-1/2/3-EXT2-2708-V1.0	MEXMRS_2708	MEXMRS_3151	02.01.2011	Solar Conjunction
MEX-X-MRS-1/2/3-EXT2-2709-V1.0	MEXMRS_2709	MEXMRS_3152	02.01.2011	Solar Conjunction
MEX-X-MRS-1/2/3-EXT2-2710-V1.0	MEXMRS_2710	MEXMRS_3153	03.01.2011	Solar Conjunction
MEX-X-MRS-1/2/3-EXT2-2711-V1.0	MEXMRS_2711	MEXMRS_3154	03.01.2011	Solar Conjunction
MEX-X-MRS-1/2/3-EXT2-2712-V1.0	MEXMRS_2712	MEXMRS_3155	04.01.2011	Solar Conjunction
MEX-X-MRS-1/2/3-EXT2-2713-V1.0	MEXMRS_2713	MEXMRS_3156	06.01.2011	Solar Conjunction
MEX-X-MRS-1/2/3-EXT2-2714-V1.0	MEXMRS_2714	MEXMRS_3157	07.01.2011	Solar Conjunction
MEX-X-MRS-1/2/3-EXT2-2715-V1.0	MEXMRS_2715	MEXMRS_3158	08.01.2011	Solar Conjunction
MEX-X-MRS-1/2/3-EXT2-2716-V1.0	MEXMRS_2716	MEXMRS_3159	08.01.2011	Solar Conjunction
MEX-X-MRS-1/2/3-EXT2-2717-V1.0	MEXMRS_2717	MEXMRS_3160	09.01.2011	Solar Conjunction
MEX-X-MRS-1/2/3-EXT2-2718-V1.0	MEXMRS_2718	MEXMRS_3161	09.01.2011	Solar Conjunction
MEX-X-MRS-1/2/3-EXT2-2721-V1.0	MEXMRS_2721	MEXMRS_3162	12.01.2011	Solar Conjunction
MEX-X-MRS-1/2/3-EXT2-2722-V1.0	MEXMRS_2722	MEXMRS_3163	13.01.2011	Solar Conjunction
MEX-X-MRS-1/2/3-EXT2-2723-V1.0	MEXMRS_2723	MEXMRS_3164	14.01.2011	Solar Conjunction
MEX-X-MRS-1/2/3-EXT2-2725-V1.0	MEXMRS_2725	MEXMRS_3165	15.01.2011	Solar Conjunction
MEX-X-MRS-1/2/3-EXT2-2727-V1.0	MEXMRS_2727	MEXMRS_3166	16.01.2011	Solar Conjunction
MEX-X-MRS-1/2/3-EXT2-2728-V1.0	MEXMRS_2728	MEXMRS_3167	17.01.2011	Solar Conjunction
MEX-X-MRS-1/2/3-EXT2-2730-V1.0	MEXMRS_2730	MEXMRS_3168	19.01.2011	Solar Conjunction
MEX-X-MRS-1/2/3-EXT2-2731-V1.0	MEXMRS_2731	MEXMRS_3169	20.01.2011	Solar Conjunction
MEX-X-MRS-1/2/3-EXT2-2733-V1.0	MEXMRS_2733	MEXMRS_3170	21.01.2011	Solar Conjunction
MEX-X-MRS-1/2/3-EXT2-2734-V1.0	MEXMRS_2734	MEXMRS_3171	22.01.2011	Solar Conjunction
	MEXMRS_2736	MEXMRS_3172	23.01.2011	Solar Conjunction
MEX-X-MRS-1/2/3-EXT2-2738-V1.0	MEXMRS_2738	MEXMRS_3173	24.01.2011	Solar Conjunction
MEX-X-MRS-1/2/3-EXT2-2740-V1.0	MEXMRS_2740	MEXMRS_3174	26.01.2011	Solar Conjunction
MEX-X-MRS-1/2/3-EXT2-2741-V1.0	MEXMRS_2741	MEXMRS_3175	27.01.2011	Solar Conjunction
MEX-X-MRS-1/2/3-EXT2-2743-V1.0	MEXMRS_2743	MEXMRS_3176	28.01.2011	Solar Conjunction
MEX-X-MRS-1/2/3-EXT2-2745-V1.0	MEXMRS_2745	MEXMRS_3177	29.01.2011	Solar Conjunction
MEX-X-MRS-1/2/3-EXT2-2747-V1.0	MEXMRS_2747	MEXMRS_3178	30.01.2011	Solar Conjunction
MEX-X-MRS-1/2/3-EXT2-2748-V1.0	MEXMRS_2748	MEXMRS_3179	30.01.2011	Solar Conjunction
MEX-X-MRS-1/2/3-EXT2-2750-V1.0	MEXMRS_2750	MEXMRS_3180	31.01.2011	Solar Conjunction
MEX-X-MRS-1/2/3-EXT2-2752-V1.0	MEXMRS_2752	MEXMRS_3181	01.02.2011	Solar Conjunction
MEX-X-MRS-1/2/3-EXT2-2756-V1.0	MEXMRS_2756	MEXMRS_3182	04.02.2011	Solar Conjunction
MEX-X-MRS-1/2/3-EXT2-2759-V1.0	MEXMRS_2759	MEXMRS_3183	06.02.2011	Solar Conjunction

MEX-X-MRS-1/2/3-EXT2-2760-V1.0	MEXMRS_2760	MEXMRS_3184	06.02.2011	Solar Conjunction
MEX-X-MRS-1/2/3-EXT2-2762-V1.0	MEXMRS_2762	MEXMRS_3185	07.02.2011	Solar Conjunction
MEX-X-MRS-1/2/3-EXT2-2763-V1.0	MEXMRS_2763	MEXMRS_3186	08.02.2011	Solar Conjunction
MEX-X-MRS-1/2/3-EXT2-2764-V1.0	MEXMRS_2764	MEXMRS_3187	09.02.2011	Solar Conjunction
MEX-X-MRS-1/2/3-EXT2-2766-V1.0	MEXMRS_2766	MEXMRS_3188	10.02.2011	Solar Conjunction
MEX-X-MRS-1/2/3-EXT2-2768-V1.0	MEXMRS_2768	MEXMRS_3189	11.02.2011	Solar Conjunction
MEX-X-MRS-1/2/3-EXT2-2769-V1.0	MEXMRS_2769	MEXMRS_3190	11.02.2011	Solar Conjunction
MEX-X-MRS-1/2/3-EXT2-2771-V1.0	MEXMRS_2771	MEXMRS_3191	11.02.2011	Solar Conjunction
MEX-X-MRS-1/2/3-EXT2-2772-V1.0	MEXMRS_2772	MEXMRS_3192	12.02.2011	Solar Conjunction
MEX-X-MRS-1/2/3-EXT2-2774-V1.0	MEXMRS_2774	MEXMRS_3193	13.02.2011	Solar Conjunction
MEX-X-MRS-1/2/3-EXT2-2775-V1.0	MEXMRS_2775	MEXMRS_3194	13.02.2011	Solar Conjunction
MEX-X-MRS-1/2/3-EXT2-2776-V1.0	MEXMRS_2776	MEXMRS_3195	14.02.2011	Solar Conjunction
MEX-X-MRS-1/2/3-EXT2-2777-V1.0	MEXMRS_2777	MEXMRS_3196	15.02.2011	Solar Conjunction
MEX-X-MRS-1/2/3-EXT2-2778-V1.0	MEXMRS_2778	MEXMRS_3197	15.02.2011	Solar Conjunction
MEX-X-MRS-1/2/3-EXT2-2779-V1.0	MEXMRS_2779	MEXMRS_3198	15.02.2011	Solar Conjunction
MEX-X-MRS-1/2/3-EXT2-2780-V1.0	MEXMRS_2780	MEXMRS_3199	16.02.2011	Solar Conjunction
MEX-X-MRS-1/2/3-EXT2-2781-V1.0	MEXMRS_2781	MEXMRS_3200	17.02.2011	Solar Conjunction
MEX-X-MRS-1/2/3-EXT2-2784-V1.0	MEXMRS_2784	MEXMRS_3201	18.02.2011	Solar Conjunction
MEX-X-MRS-1/2/3-EXT2-2785-V1.0	MEXMRS_2785	MEXMRS_3202	19.02.2011	Solar Conjunction
MEX-X-MRS-1/2/3-EXT2-2786-V1.0	MEXMRS_2786	MEXMRS_3203	20.02.2011	Solar Conjunction
MEX-X-MRS-1/2/3-EXT2-2789-V1.0	MEXMRS_2789	MEXMRS_3204	22.02.2011	Solar Conjunction
MEX-X-MRS-1/2/3-EXT2-2790-V1.0	MEXMRS_2790	MEXMRS_3205	23.02.2011	Solar Conjunction
MEX-X-MRS-1/2/3-EXT2-2791-V1.0	MEXMRS_2791	MEXMRS_3206	24.02.2011	Solar Conjunction
MEX-X-MRS-1/2/3-EXT2-2792-V1.0	MEXMRS_2792	MEXMRS_3207	25.02.2011	Solar Conjunction
MEX-X-MRS-1/2/3-EXT2-2794-V1.0	MEXMRS_2794	MEXMRS_3208	26.02.2011	Solar Conjunction
MEX-X-MRS-1/2/3-EXT2-2795-V1.0	MEXMRS_2795	MEXMRS_3209	27.02.2011	Solar Conjunction
MEX-X-MRS-1/2/3-EXT2-2797-V1.0	MEXMRS_2797	MEXMRS_3210	28.02.2011	Solar Conjunction
MEX-X-MRS-1/2/3-EXT2-2798-V1.0	MEXMRS_2798	MEXMRS_3211	01.03.2011	Solar Conjunction
MEX-X-MRS-1/2/3-EXT2-2799-V1.0	MEXMRS_2799	MEXMRS_3212	02.03.2011	Solar Conjunction
MEX-X-MRS-1/2/3-EXT2-2800-V1.0	MEXMRS_2800	MEXMRS_3213	02.03.2011	Solar Conjunction
MEX-X-MRS-1/2/3-EXT2-2801-V1.0	MEXMRS_2801	MEXMRS_3214	03.03.2011	Solar Conjunction
MEX-X-MRS-1/2/3-EXT2-2802-V1.0	MEXMRS_2802	MEXMRS_3215	04.03.2011	Solar Conjunction
MEX-X-MRS-1/2/3-EXT2-2803-V1.0	MEXMRS_2803	MEXMRS_3216	04.03.2011	Solar Conjunction
MEX-X-MRS-1/2/3-EXT2-2804-V1.0	MEXMRS_2804	MEXMRS_3217	05.03.2011	Solar Conjunction
MEX-X-MRS-1/2/3-EXT2-2805-V1.0	MEXMRS_2805	MEXMRS_3218	06.03.2011	Solar Conjunction

MEX-X-MRS-1/2/3-EXT2-2806-V1.0	MEXMRS_2806	MEXMRS_3219	07.03.2011	Solar Conjunction
MEX-X-MRS-1/2/3-EXT2-2807-V1.0	MEXMRS_2807	MEXMRS_3220	08.03.2011	Solar Conjunction
MEX-X-MRS-1/2/3-EXT2-2808-V1.0	MEXMRS_2808	MEXMRS_3221	08.03.2011	Solar Conjunction
MEX-X-MRS-1/2/3-EXT2-2809-V1.0	MEXMRS_2809	MEXMRS_3222	08.03.2011	Solar Conjunction
MEX-X-MRS-1/2/3-EXT2-2810-V1.0	MEXMRS_2810	MEXMRS_3223	09.03.2011	Solar Conjunction
MEX-X-MRS-1/2/3-EXT2-2811-V1.0	MEXMRS_2811	MEXMRS_3224	10.03.2011	Solar Conjunction
MEX-X-MRS-1/2/3-EXT2-2812-V1.0	MEXMRS_2812	MEXMRS_3225	11.03.2011	Solar Conjunction
MEX-X-MRS-1/2/3-EXT2-2813-V1.0	MEXMRS_2813	MEXMRS_3226	11.03.2011	Solar Conjunction
MEX-X-MRS-1/2/3-EXT2-2814-V1.0	MEXMRS_2814	MEXMRS_3227	12.03.2011	Solar Conjunction
MEX-X-MRS-1/2/3-EXT2-2815-V1.0	MEXMRS_2815	MEXMRS_3228	13.03.2011	Solar Conjunction
MEX-X-MRS-1/2/3-EXT2-2816-V1.0	MEXMRS_2816	MEXMRS_3229	13.03.2011	Solar Conjunction
MEX-X-MRS-1/2/3-EXT2-2817-V1.0	MEXMRS_2817	MEXMRS_3230	14.03.2011	Solar Conjunction
MEX-X-MRS-1/2/3-EXT2-2818-V1.0	MEXMRS_2818	MEXMRS_3231	15.03.2011	Solar Conjunction
MEX-X-MRS-1/2/3-EXT2-2819-V1.0	MEXMRS_2819	MEXMRS_3232	15.03.2011	Solar Conjunction
MEX-X-MRS-1/2/3-EXT2-2820-V1.0	MEXMRS_2820	MEXMRS_3233	16.03.2011	Solar Conjunction
MEX-X-MRS-1/2/3-EXT2-2821-V1.0	MEXMRS_2821	MEXMRS_3234	17.03.2011	Solar Conjunction
MEX-X-MRS-1/2/3-EXT2-2822-V1.0	MEXMRS_2822	MEXMRS_3235	18.03.2011	Solar Conjunction
MEX-X-MRS-1/2/3-EXT2-2823-V1.0	MEXMRS_2823	MEXMRS_3236	19.03.2011	Solar Conjunction
MEX-X-MRS-1/2/3-EXT2-2824-V1.0	MEXMRS_2824	MEXMRS_3237	19.03.2011	Solar Conjunction
MEX-X-MRS-1/2/3-EXT2-2825-V1.0	MEXMRS_2825	MEXMRS_3238	23.03.2011	Solar Conjunction
MEX-X-MRS-1/2/3-EXT2-2826-V1.0	MEXMRS_2826	MEXMRS_3239	24.03.2011	Solar Conjunction
MEX-X-MRS-1/2/3-EXT2-2827-V1.0	MEXMRS_2827	MEXMRS_3240	24.03.2011	Solar Conjunction
MEX-X-MRS-1/2/3-EXT2-2828-V1.0	MEXMRS_2828	MEXMRS_3241	25.03.2011	Solar Conjunction
MEX-X-MRS-1/2/3-EXT2-2829-V1.0	MEXMRS_2829	MEXMRS_3242	26.03.2011	Solar Conjunction
MEX-X-MRS-1/2/3-EXT2-2830-V1.0	MEXMRS_2830	MEXMRS_3243	26.03.2011	Solar Conjunction
MEX-X-MRS-1/2/3-EXT2-2831-V1.0	MEXMRS_2831	MEXMRS_3244	27.03.2011	Solar Conjunction

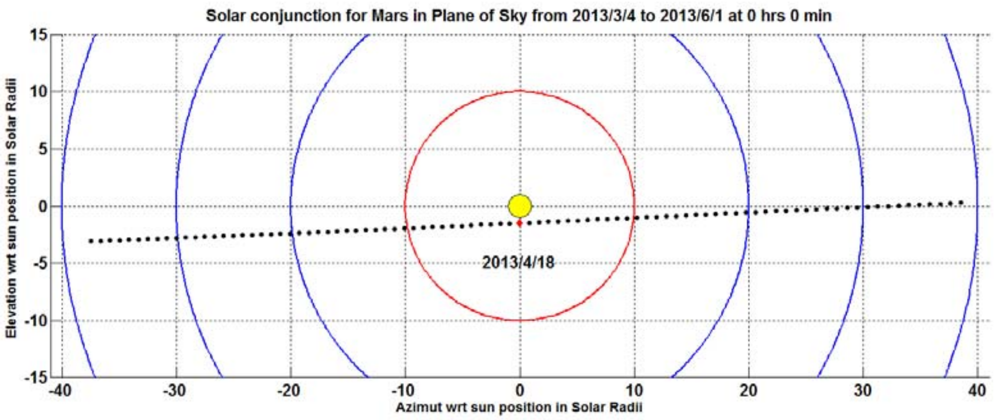

Fig. 37. : MEX SCO 2013 plane of sky plot. The position of MEX is shown for each day in the solar offset range between +/- 40 solar radii. The central red dot marks the date of solar conjunction.

PSA Dataset Name	RSI Volume ID	Volume ID	Start Date	Notes
MEX-X-MRS-1/2/3-EXT2-3476-V1.0	MEXMRS_3476	MEXMRS_3256	04.03.2013	Solar Conjunction
MEX-X-MRS-1/2/3-EXT2-3477-V1.0	MEXMRS_3477	MEXMRS_3257	05.03.2013	Solar Conjunction
MEX-X-MRS-1/2/3-EXT2-3478-V1.0	MEXMRS_3478	MEXMRS_3258	08.03.2013	Solar Conjunction
MEX-X-MRS-1/2/3-EXT2-3480-V1.0	MEXMRS_3480	MEXMRS_3260	12.03.2013	Solar Conjunction
MEX-X-MRS-1/2/3-EXT2-3481-V1.0	MEXMRS_3481	MEXMRS_3261	13.03.2013	Solar Conjunction
MEX-X-MRS-1/2/3-EXT2-3482-V1.0	MEXMRS_3482	MEXMRS_3262	15.03.2013	Solar Conjunction
MEX-X-MRS-1/2/3-EXT2-3484-V1.0	MEXMRS_3484	MEXMRS_3259	11.03.2013	Solar Conjunction
MEX-X-MRS-1/2/3-EXT2-3485-V1.0	MEXMRS_3485	MEXMRS_3263	17.03.2013	Solar Conjunction
MEX-X-MRS-1/2/3-EXT2-3486-V1.0	MEXMRS_3486	MEXMRS_3264	18.03.2013	Solar Conjunction
MEX-X-MRS-1/2/3-EXT2-3487-V1.0	MEXMRS_3487	MEXMRS_3265	20.03.2013	Solar Conjunction
MEX-X-MRS-1/2/3-EXT2-3523-V1.0	MEXMRS_3523	MEXMRS_3282	05.05.2013	Solar Conjunction
MEX-X-MRS-1/2/3-EXT2-3524-V1.0	MEXMRS_3524	MEXMRS_3283	12.05.2013	Solar Conjunction
MEX-X-MRS-1/2/3-EXT2-3525-V1.0	MEXMRS_3525	MEXMRS_3284	13.05.2013	Solar Conjunction
MEX-X-MRS-1/2/3-EXT2-3526-V1.0	MEXMRS_3526	MEXMRS_3285	17.05.2013	Solar Conjunction
MEX-X-MRS-1/2/3-EXT2-3527-V1.0	MEXMRS_3527	MEXMRS_3286	19.05.2013	Solar Conjunction
MEX-X-MRS-1/2/3-EXT2-3533-V1.0	MEXMRS_3533	MEXMRS_3266	01.04.2013	Solar Conjunction
MEX-X-MRS-1/2/3-EXT2-3534-V1.0	MEXMRS_3534	MEXMRS_3267	02.04.2013	Solar Conjunction
MEX-X-MRS-1/2/3-EXT2-3535-V1.0	MEXMRS_3535	MEXMRS_3268	05.04.2013	Solar Conjunction
MEX-X-MRS-1/2/3-EXT2-3536-V1.0	MEXMRS_3536	MEXMRS_3269	06.04.2013	Solar Conjunction
MEX-X-MRS-1/2/3-EXT2-3538-V1.0	MEXMRS_3538	MEXMRS_3270	07.04.2013	Solar Conjunction
MEX-X-MRS-1/2/3-EXT2-3540-V1.0	MEXMRS_3540	MEXMRS_3271	09.04.2013	Solar Conjunction

MEX-X-MRS-1/2/3-EXT2-3545-V1.0	MEXMRS_3545	MEXMRS_3272	13.04.2013	Solar Conjunction
MEX-X-MRS-1/2/3-EXT2-3574-V1.0	MEXMRS_3574	MEXMRS_3278	27.04.2013	Solar Conjunction
MEX-X-MRS-1/2/3-EXT2-3575-V1.0	MEXMRS_3575	MEXMRS_3279	29.04.2013	Solar Conjunction
MEX-X-MRS-1/2/3-EXT2-3576-V1.0	MEXMRS_3576	MEXMRS_3280	30.04.2013	Solar Conjunction
MEX-X-MRS-1/2/3-EXT2-3577-V1.0	MEXMRS_3577	MEXMRS_3281	01.05.2013	Solar Conjunction
MEX-X-MRS-1/2/3-EXT2-3578-V1.0	MEXMRS_3578	MEXMRS_3287	26.05.2013	Solar Conjunction
MEX-X-MRS-1/2/3-EXT2-3579-V1.0	MEXMRS_3579	MEXMRS_3288	27.05.2013	Solar Conjunction
MEX-X-MRS-1/2/3-EXT2-3580-V1.0	MEXMRS_3580	MEXMRS_3289	29.05.2013	Solar Conjunction
MEX-X-MRS-1/2/3-EXT2-3581-V1.0	MEXMRS_3581	MEXMRS_3290	30.05.2013	Solar Conjunction
MEX-X-MRS-1/2/3-EXT2-3582-V1.0	MEXMRS_3582	MEXMRS_3291	31.05.2013	Solar Conjunction

- **ROS SCO 2006**

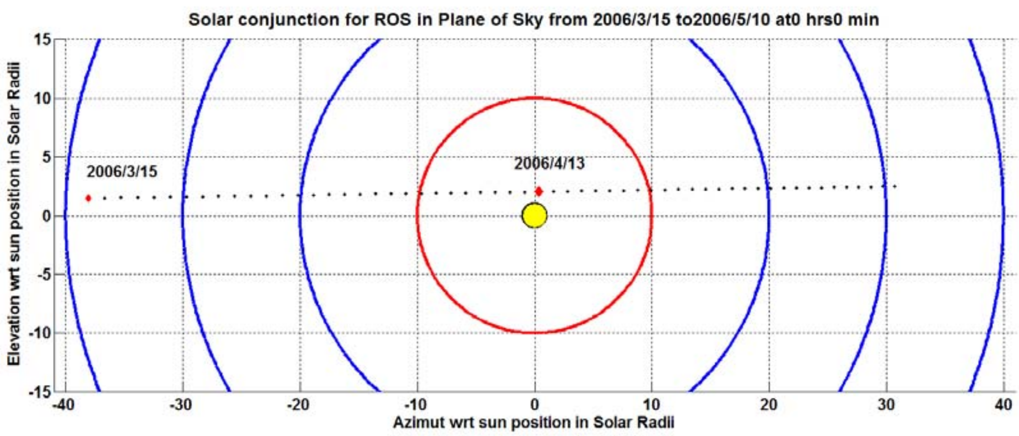

Fig. 38. ROS SCO 2006 plane of sky plot (similar to Fig. 33).

The list below is extracted from the aareadme.txt file of the Rosetta folder ftp://psa.esac.esa.int/pub/mirror/INTERNATIONAL-ROSETTA-MISSION/RSI/ and reflects the archived data until:

PUBLICATION_DATE = 2012-03-02

PSA Dataset Name	RSI Volume ID	Volume ID	Start Date	Notes
RO-X-RSI-1/2/3-CR2-0015-V1.0	RORSI_0015	RORSI_3001	02.03.2006	Solar Conjunction
RO-X-RSI-1/2/3-CR2-0016-V1.0	RORSI_0016	RORSI_3021	15.03.2006	Solar Conjunction
RO-X-RSI-1/2/3-CR2-0017-V1.0	RORSI_0017	RORSI_3007	16.03.2006	Solar Conjunction

RO-X-RSI-1/2/3-CR2-0018-V1.0	RORSI_0018	RORSI_3002	22.03.2006	Solar Conjunction
RO-X-RSI-1/2/3-CR2-0019-V1.0	RORSI_0019	RORSI_3003	23.03.2006	Solar Conjunction
RO-X-RSI-1/2/3-CR2-0020-V1.0	RORSI_0020	RORSI_3004	24.03.2006	Solar Conjunction
RO-X-RSI-1/2/3-CR2-0021-V1.0	RORSI_0021	RORSI_3005	28.03.2006	Solar Conjunction
RO-X-RSI-1/2/3-CR2-0022-V1.0	RORSI_0022	RORSI_3006	29.03.2006	Solar Conjunction
RO-X-RSI-1/2/3-CR2-0023-V1.0	RORSI_0023	RORSI_3008	30.03.2006	Solar Conjunction
RO-X-RSI-1/2/3-CR2-0024-V1.0	RORSI_0024	RORSI_3009	31.03.2006	Solar Conjunction
RO-X-RSI-1/2/3-CR2-0025-V1.0	RORSI_0025	RORSI_3010	01.04.2006	Solar Conjunction
RO-X-RSI-1/2/3-CR2-0026-V1.0	RORSI_0026	RORSI_3011	04.04.2006	Solar Conjunction
RO-X-RSI-1/2/3-CR2-0027-V1.0	RORSI_0027	RORSI_3024	05.04.2006	Solar Conjunction
RO-X-RSI-1/2/3-CR2-0028-V1.0	RORSI_0028	RORSI_3012	06.04.2006	Solar Conjunction
RO-X-RSI-1/2/3-CR2-0029-V1.0	RORSI_0029	RORSI_3013	07.04.2006	Solar Conjunction
RO-X-RSI-1/2/3-CR2-0030-V1.0	RORSI_0030	RORSI_3014	08.04.2006	Solar Conjunction
RO-X-RSI-1/2/3-CR2-0031-V1.0	RORSI_0031	RORSI_3015	10.04.2006	Solar Conjunction
RO-X-RSI-1/2/3-CR2-0032-V1.0	RORSI_0032	RORSI_3025	15.04.2006	Solar Conjunction
RO-X-RSI-1/2/3-CR2-0033-V1.0	RORSI_0033	RORSI_3026	16.04.2006	Solar Conjunction
RO-X-RSI-1/2/3-CR2-0034-V1.0	RORSI_0034	RORSI_3027	17.04.2006	Solar Conjunction
RO-X-RSI-1/2/3-CR2-0035-V1.0	RORSI_0050	RORSI_3040	09.05.2006	Solar Conjunction
RO-X-RSI-1/2/3-CR2-0036-V1.0	RORSI_0036	RORSI_3029	19.04.2006	Solar Conjunction
RO-X-RSI-1/2/3-CR2-0037-V1.0	RORSI_0037	RORSI_3016	20.04.2006	Solar Conjunction
RO-X-RSI-1/2/3-CR2-0038-V1.0	RORSI_0038	RORSI_3030	21.04.2006	Solar Conjunction
RO-X-RSI-1/2/3-CR2-0039-V1.0	RORSI_0039	RORSI_3031	22.04.2006	Solar Conjunction
RO-X-RSI-1/2/3-CR2-0040-V1.0	RORSI_0040	RORSI_3017	23.04.2006	Solar Conjunction
RO-X-RSI-1/2/3-CR2-0041-V1.0	RORSI_0041	RORSI_3018	24.04.2006	Solar Conjunction
RO-X-RSI-1/2/3-CR2-0042-V1.0	RORSI_0042	RORSI_3032	25.04.2006	Solar Conjunction
RO-X-RSI-1/2/3-CR2-0043-V1.0	RORSI_0043	RORSI_3019	26.04.2006	Solar Conjunction
RO-X-RSI-1/2/3-CR2-0044-V1.0	RORSI_0044	RORSI_3020	27.04.2006	Solar Conjunction
RO-X-RSI-1/2/3-CR2-0045-V1.0	RORSI_0051	RORSI_3041	10.05.2006	Solar Conjunction
RO-X-RSI-1/2/3-CR2-0046-V1.0	RORSI_0046	RORSI_3022	29.04.2006	Solar Conjunction
RO-X-RSI-1/2/3-CR2-0047-V1.0	RORSI_0047	RORSI_3038	02.05.2006	Solar Conjunction
RO-X-RSI-1/2/3-CR2-0048-V1.0	RORSI_0048	RORSI_3039	03.05.2006	Solar Conjunction
RO-X-RSI-1/2/3-CR2-0049-V1.0	RORSI_0049	RORSI_3023	04.05.2006	Solar Conjunction
RO-X-RSI-1/2/3-CR2-0050-V1.0	RORSI_0050	RORSI_3040	09.05.2006	Solar Conjunction
RO-X-RSI-1/2/3-CR2-0051-V1.0	RORSI_0051	RORSI_3041	10.05.2006	Solar Conjunction
RO-X-RSI-1/2/3-CR2-0120-V1.0	RORSI_0120	RORSI_6001	11.04.2006	Solar Conjunction

RO-X-RSI-1/2/3-CR2-0121-V1.0	RORSI_0121	RORSI_3028	12.04.2006	Solar Conjunction
RO-X-RSI-1/2/3-CR2-0122-V1.0	RORSI_0122	RORSI_3034	13.04.2006	Solar Conjunction
RO-X-RSI-1/2/3-CR2-0123-V1.0	RORSI_0123	RORSI_3035	14.04.2006	Solar Conjunction

B. Processing steps on the Doppler residuals

The calculation of the Doppler predict "*predicted received antenna frequency Doppler*" of the level 2 dataset is based on the reconstructed orbit file and the DE405 ephemeris. For the calculation the radio science team software has to model the path and movement effects similar to the FD software which were used for the computation of the reconstructed orbit file. A summary of the effects that are taken into account in that radio science team software package are described in ref RD 19.

Anyhow, because the reconstructed orbit has not corrected for the corona plasma content, the mean slow increase of plasma content in each tracking pass is part of the orbit. The radio science software used for the calculation of the predicted received antenna Doppler frequency has applied the same approach. Therefore the mean difference of the Doppler residuals between both (measured and calculated) should be zero.

The level 2 residual calibrated frequency shift as shown in Fig. 25 has an offset of 70 – 100 mHz and compared with the integrated differential Doppler residuals also the shape over time is different. This means, that the residual calibrated frequency shifts can not be used for the calculation of the TEC at this point of the analysis. Further processing is needed and possible steps are described below after the summary of the steps that are involved to get these residuals.

Summary: Processing steps that are involved in order to get the residual calibrated frequency shifts (the steps written in *italic* format are computed by FD and those with the normal format by RS):

- the starting point of the processing are the measured received x-band frequency values
- *the X-Band values of the received signal are corrected for the earth neutral Atmosphere and Ionosphere and others (see chapter 4.8).*
- *the corrected values are then used to reconstruct (find) the orbit that produces the smallest deviation between the received Doppler values and the calculated Doppler values for the data arcs (RD 33, RD 34)*

RS gets the reconstructed orbit file (the FD Doppler residuals between received and calculated values from the reconstructed orbit file are not available and because some parts of the FD calculations are not published in detail the residuals are somehow part of the error of the TEC calculation on the uplink in a 2 way 2 frequency experiment configuration. Anyhow, no error will remain in the differential downlink values also for one frequency values the error for relatively fast changing plasma components will be negligible, because these plasma changes are not part of the reconstructed orbit and a baseline fit on the residuals reduces the effect of remaining movements that are still part of the residuals.

(The following steps are not needed for the calculation of the diff Doppler residuals)
- RS computes the received frequency by applying the reconstructed orbit file
- the calculated Doppler values are then corrected for the earth atmosphere and Ionosphere effects on the uplink and downlink
- and we get the predicted received sky frequency

- measured frequency – predicted frequency = 2 way x-band Doppler residuals (residual calibrated frequency shifts of the level 2 data column 12)

In the following some possible steps are summarized that can be applied on the level 2 "residual calibrated frequency shifts" that may give the Doppler residuals due to the TEC on the uplink (in case differential ranging data is available the absolute value of the TEC has to be taken into account and the procedure has to be adapted)

- adjust the differential Doppler downlink values to the x-band downlink frequency (multiply the Doppler residua with the constant value as given in equation (3.26))
- subtract the frequency adjusted diff Dop residua (step 1) from the x-band downlink 2-way residuals
- do a baseline-fit on the remaining residuals with a low order polynomial. The remaining residuals are the sum of the "fast" changing plasma components and parts of the slowly changing mean TEC on the uplink but converted to a downlink frequency shift
- compare the phase (or TEC) values of the adjusted diff Doppler x-band downlink with the phase values of the remaining adjusted residuals of the uplink. Due to the 2nd order polynomial baseline fit some parts of the plasma on the uplink are lost.

  For further calculations:

  <u>Usage of unaffected (fast changing) features</u>
- use a LP-filter on both phase (integrated Doppler) residual datasets to take off the fast changes that are shown on a scale of approx. 5 min periods.
- use a HP-filter to take off the constant and slowly changing terms up to a period of approx 2h. These residuals can also be achieved with a second LP- Filter and a calculation of the difference between the 2 filtered signals. (Maybe some tests have to be done to get the final bandwidths)
- the remaining residuals are big enough in duration to show no changes during the travel time between the uplink and downlink path and are not much affected due to the orbit or the baseline fit. These residuals might give the best results on the velocity calculation.
- do a correlation between parts of the data in order to get the time offset between up- and downlink (see chapter 3.5)